

A REVISED MODEL FOR THE FORMATION OF DISK GALAXIES: LOW SPIN AND DARK-HALO EXPANSION

AARON A. DUTTON

Department of Physics, Swiss Federal Institute of Technology (ETH Zurich), CH-8093 Zurich, Switzerland

FRANK C. VAN DEN BOSCH

Max-Planck-Institut für Astronomie, Königstuhl 17, 69117 Heidelberg, Germany

AVISHAI DEKEL

Racah Institute of Physics, The Hebrew University, Jerusalem, Israel

AND

STÉPHANE COURTEAU

Department of Physics, Eng. Physics & Astronomy, Queen's University, Kingston, ON K7L 3N6, Canada

THE ASTROPHYSICAL JOURNAL 654:27-52, 2007 January 1

ABSTRACT

We use observed rotation velocity-luminosity (*VL*) and size-luminosity (*RL*) relations to single out a specific scenario for disk galaxy formation in the Λ CDM cosmology. Our model involves four independent log-normal random variables: dark-halo concentration c , disk spin λ_{gal} , disk mass fraction m_{gal} , and stellar mass-to-light ratio Υ_1 . A simultaneous match of the *VL* and *RL* zero points with adiabatic contraction requires low- c halos, but this model has $V_{2.2} \sim 1.8V_{\text{vir}}$ (where $V_{2.2}$ and V_{vir} are the circular velocity at 2.2 disk scale lengths and the virial radius, respectively) which will be unable to match the luminosity function (LF). Similarly models without adiabatic contraction but standard c also predict high values of $V_{2.2}/V_{\text{vir}}$. Models in which disk formation induces an *expansion* rather than the commonly assumed contraction of the dark-matter halos have $V_{2.2} \sim 1.2V_{\text{vir}}$ which allows a simultaneous fit of the LF. This may result from non-spherical, clumpy gas accretion, where dynamical friction transfers energy from the gas to the dark matter. This model requires low λ_{gal} and m_{gal} values, contrary to naive expectations. However, the low λ_{gal} is consistent with the notion that disk galaxies predominantly survive in halos with a quiet merger history, while a low m_{gal} is also indicated by galaxy-galaxy lensing. The smaller than expected scatter in the *RL* relation, and the lack of correlation between the residuals of the *VL* and *RL* relations, respectively, imply that the scatter in λ_{gal} and in c need to be smaller than predicted for Λ CDM halos, again consistent with the idea that disk galaxies preferentially reside in halos with a quiet merger history.

Subject headings: galaxies: formation — galaxies: fundamental parameters — galaxies: spiral — galaxies: structure

1. INTRODUCTION

In the standard, cold dark matter (CDM) based model for disk formation, set out by Fall & Efstathiou (1980), disks form out of gas that slowly cools out of a hot gaseous halo, associated with the dark matter potential well, while maintaining its specific angular momentum. During this process the dark matter halo contracts to conserve its adiabatic invariants (Blumenthal et al. 1986). Because of the centrifugal barrier the gas settles in a rotationally supported disk whose size is proportional to both the size and angular momentum of the dark matter halo (Mo, Mao & White, 1998; hereafter MMW). Consequently, the structure and dynamics of disk galaxies are expected to be strongly correlated with the properties of their dark matter halos. In particular, the correlations between the observable, structural parameters of disk galaxies, rotation velocity, V , size, R , and luminosity, L , are expected to be a reflection of the virial properties of dark matter halos, which scale as $V_{\text{vir}} \propto R_{\text{vir}} \propto M_{\text{vir}}^{1/3}$. Slight deviations from these scalings are expected from the fact that more massive halos are, on average, less concentrated. Any further deviations must either reflect some aspects of the baryonic physics related to galaxy formation, or signal a failure in the standard picture outlined

above. In what follows we refer to the relations between the global disk parameters as the *VL*, *RL*, and *RV* relations.

In the past, the *VL* relation, also known as the Tully-Fisher relation (Tully & Fisher 1977), has received much attention as a distance indicator owing to the relatively small observed scatter. Although numerous studies have addressed the origin of the *VL* relation, no consensus has been reached. In particular, it is currently still under debate whether the origin of the *VL* relation is mainly governed by initial cosmological conditions (e.g., Eisenstein & Loeb 1996; Avila-Reese, Firmani & Hernández 1998), or by the detailed processes governing star formation (Silk 1997; Heavens & Jiminez 1999) and/or feedback (e.g., Kauffmann, White & Guiderdoni 1993; Cole et al. 1994; Elizondo et al. 1999; Natarajan 1999). In the most recent models (van den Bosch 2000; 2002; Navarro & Steinmetz 2000; Firmani & Avila-Reese 2000, hereafter FA00) it is typically understood that both initial conditions and baryonic physics related to star formation and feedback must play an important role. Reproducing the *VL* zero point has also been a long standing problem for CDM based galaxy formation models. In particular no model has been able to simultaneously match the luminosity function and *VL* zero point

using standard Λ CDM parameters (Cole et al. 2000; Benson et al. 2003; Yang, Mo, & van den Bosch 2003). This problem can be traced to the high values of V/V_{vir} expected for Λ CDM halos once the effects of the baryons, such as adiabatic contraction (Blumenthal et al. 1986), are taken into account. All solutions to this problem require a change to either the standard cosmological model or the standard picture of galaxy formation.

Another potential problem for disk formation models is the formation of large enough disks. The relative fragility of disk galaxies and the strongly ordered motion of their stars and gas is generally interpreted as evidence for a relatively smooth formation history without violent merger processes. The sub-sample of dark matter halos without recent major mergers is known to have systematically low spin parameters (D'Onghia & Burkert 2004). However, standard models for the formation of extended rotating disks seem to require high spin parameters in order to reproduce the zero point of the *RL* relation.

In addition to the slopes and zero points of the *VL* and *RL* relations, additional constraints come from the scatter in these two relations. In particular, Courteau & Rix (1999; hereafter CR99) have shown that the residuals of the *VL* relation, at fixed L , are virtually uncorrelated with the residuals of the *RL* relation, at fixed L (see also McGaugh 2005). This is another way of expressing the fact that the *VL* relation is independent of surface brightness (see Courteau et al. 2006 for details), and implies that the size of a disk at given L has no relevance to its rotation velocity. This is a puzzling result to explain, as one would naively expect that a more concentrated disk also results in a higher rotation velocity. CR99, therefore, interpreted the weak residual correlation as indicating that, *on average*, high surface brightness (HSB) disks are submaximal, so that the disk only contributes mildly to the observed rotation velocity. If confirmed this puts constraints on the stellar mass-to-light ratio, Υ , and thus on the stellar initial mass function (IMF). FA00, on the other hand, claim that the weak residual correlation owes to the surface density dependence of star formation, such that at a given baryonic mass, lower surface density galaxies have lower stellar masses, and hence lower luminosities, which compensate for the somewhat lower rotation velocities. However, in their model both the highest and lowest surface brightness galaxies lie above the mean *VL* relation, contrary to observations, and their models do not reproduce the zero point of the *VL* relation or the amount of scatter in the *VL* and *RL* relations.

Although various studies have attempted to explain the origin of the *VL* or the *RL* relation, the true challenge lies in finding a self-consistent model of disk formation that can match both relations as well as the galaxy luminosity function *simultaneously*. Finding such a model is a non-trivial task, as all current models fail to do so. In this paper we examine the parameter space of such models within the standard Λ CDM cosmology. We simultaneously match the slopes, zero points and residuals of the *VL* and *RL* relations. We also investigate what each of these models predict for the mean V/V_{vir} . In order to be able to reproduce the observed abundances of disk galaxies, this ratio needs to be relatively low ~ 1.2 . We show that this restriction severely limits the allowable parameter space, favoring a model with low spin parameter λ_{gal} , low galaxy mass fraction m_{gal} , and with halo expansion rather than halo contraction.

The key ingredients of our model are as follows:

1. Disk galaxies form in spherical dark-matter halos

whose properties are drawn from N-body simulations of the standard Λ CDM cosmology. In particular, their density profiles have an NFW form with a concentration parameter c that declines systematically with mass.

2. The baryons form an exponential disk in centrifugal equilibrium, which is specified by a mass fraction m_{gal} and a spin parameter λ_{gal} .
3. The galaxy mass fraction is treated as a free parameter with a mean $m_{\text{gal}} \propto M_{\text{vir}}^{\alpha_m}$. Positive values of α_m are expected from feedback effects.
4. A bulge is included based on a self-regulating mechanism that ensures disk stability.
5. The interaction between the baryons and the dark matter halo is modeled with a generalized adiabatic contraction model which also allows for halo expansion.
6. Stars form in the disk once above a threshold surface density.
7. The I-band stellar mass-to-light ratio Υ_I increases with luminosity as constrained by observations.
8. The model parameters c , λ_{gal} , m_{gal} and Υ_I are assumed to be independent log-normal random variables.

The data and models are introduced in §2 and §3, respectively. In §3.4 we outline the conversion between stellar mass and luminosity; In §3.5 we detail the computation of our model scaling relations. In §4 we discuss how to construct models that match the slopes, zero points, scatter and residual correlation. In §5 we explore the model parameter space, and advocate a revised model for disk formation. We summarize our results in §6.

2. THE DATA

We compare our models with the large data set of ~ 1600 local disk galaxies compiled by Courteau et al. (2006). For each of these galaxies a rotation velocity V , a luminosity L , a disk scale length R , and a central surface brightness of the disk μ_0 , are available. The data set is compiled from three independent samples: Mathewson, Ford, & Buchhorn 1992 (hereafter, MAT); Courteau et al. 2000 (hereafter, Shellflow); and Dale et al. 1999 (hereafter, SCII).

All galaxy luminosities are measured in the *I*-band, and correspond to *total* luminosities (i.e., disk plus bulge). In addition, for a significant sub-sample we also have optical colors available, which we use to estimate stellar mass-to-light ratios (see §3.4 below). Disk scale lengths and surface brightnesses are determined from the *I*-band photometry. In what follows, whenever we refer to surface brightness we mean the *central* surface brightness, $\mu_{0,I}$, of the exponential disk fitted to the data.

Due to the complications involved with interpreting H α line widths, we only use rotation velocities derived from resolved H α rotation curves. This reduces the full sample by ~ 300 galaxies. For the MAT and Shellflow samples the rotation curves are fitted with a parametric function (Courteau 1997) which is then evaluated at 2.2 disk scale lengths. For the SCII sample the velocities are measured at the optical radius (equivalent to 3.2 scale lengths for an exponential disk).

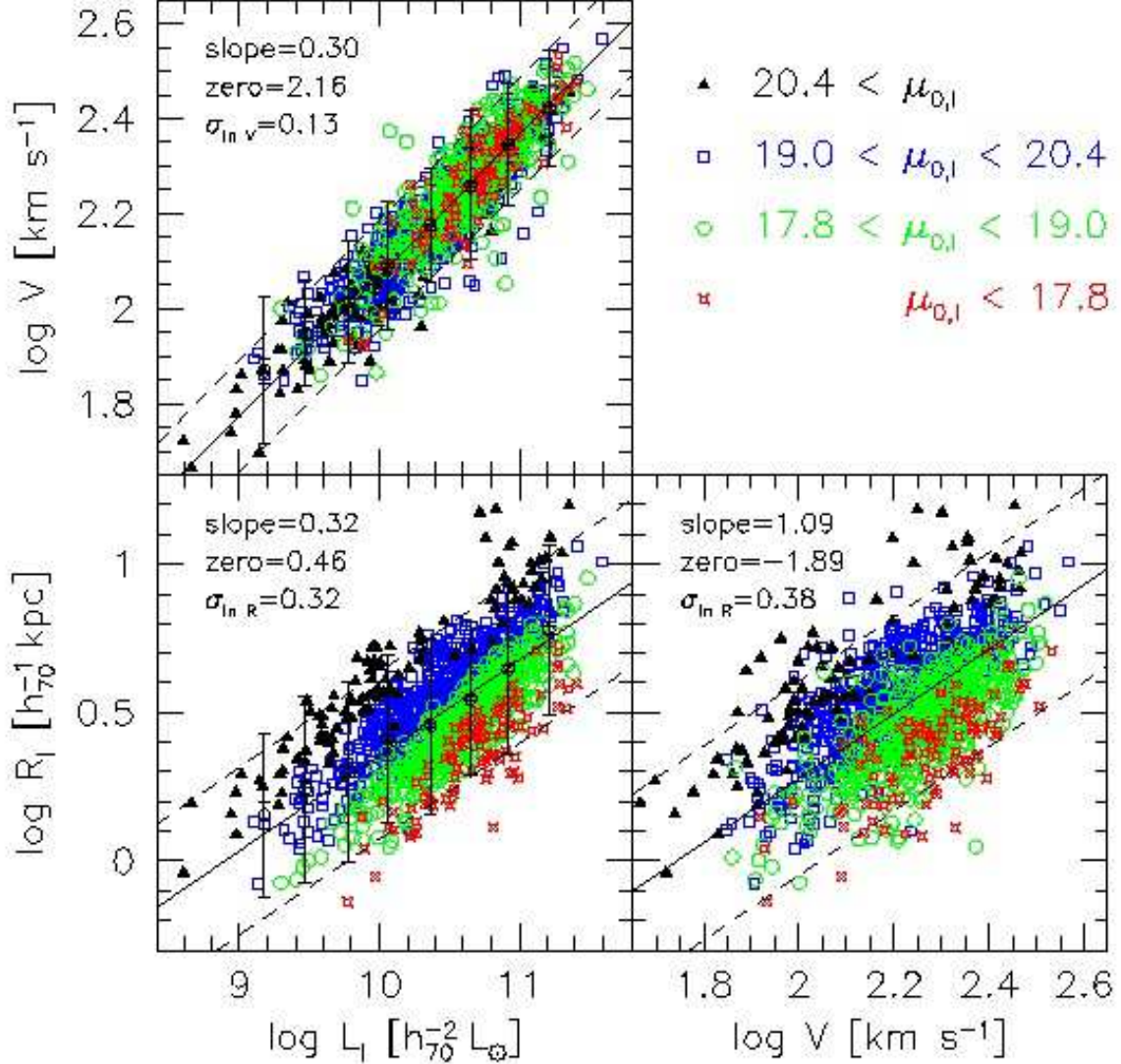


FIG. 1.— Observed I-band VLR scaling relations using data from Courteau et al. 2006. Bi-weighted orthogonal least squares fits are given by the solid black lines, with 2-sigma deviations given by the dashed lines. The open black circles with error bars show the mean and 2-sigma scatter of the VL and RL relations binned at 0.3 dex intervals in L_I . The colors and point types correspond to extrapolated disk central surface brightness, $\mu_{0,I}$ as indicated in the top right panel.

2.1. Corrections

In order to homogenize these data samples as much as possible, we have derived the inclination and cosmological corrections to the velocities, luminosities and scale lengths in a uniform way, as described below.

The observed rotation velocities, V_{obs} , are corrected for inclination and cosmological broadening using

$$V = \frac{V_{\text{obs}}}{(1+z) \sin i}. \quad (1)$$

The inclination, i , is computed using

$$\sin i = \sqrt{\frac{1-(b/a)^2}{1-q_0^2}}, \quad (2)$$

where b/a is the minor-to-major axis ratio, and q_0 is the intrinsic thickness of the disk. We assume $q_0 = 0.2$, and set $i = 90^\circ$ if $b/a < q_0$.

The apparent magnitudes, m_I , are corrected for both internal extinction, A_{int} , and external (i.e., Galactic) extinction, A_{ext} . A small k-correction, A_k , is also applied such that

$$m_I = m_{I,\text{obs}} - A_{\text{int}} - A_{\text{ext}} - A_k. \quad (3)$$

Internal extinctions are computed using the line-width ($W = 2V$) dependent relation from Tully et al. (1998):

$$A_{\text{int}} = \gamma_I(W) \log(a/b) = [0.92 + 1.63(\log W - 2.5)] \log(a/b) \quad (4)$$

with a/b the major-to-minor axis ratio. The external (Galactic) extinction is computed using the dust maps of Schlegel, Finkbeiner, & Davis (1998), while the k-corrections are computed using the line width dependent formalism of Willick et al. (1997).

The absolute magnitudes, M_I , are computed using

$$M_I = m_I - 5 \log D_L - 25; \quad D_L = \frac{V_{\text{CMB}}}{100h} (1+z), \quad (5)$$

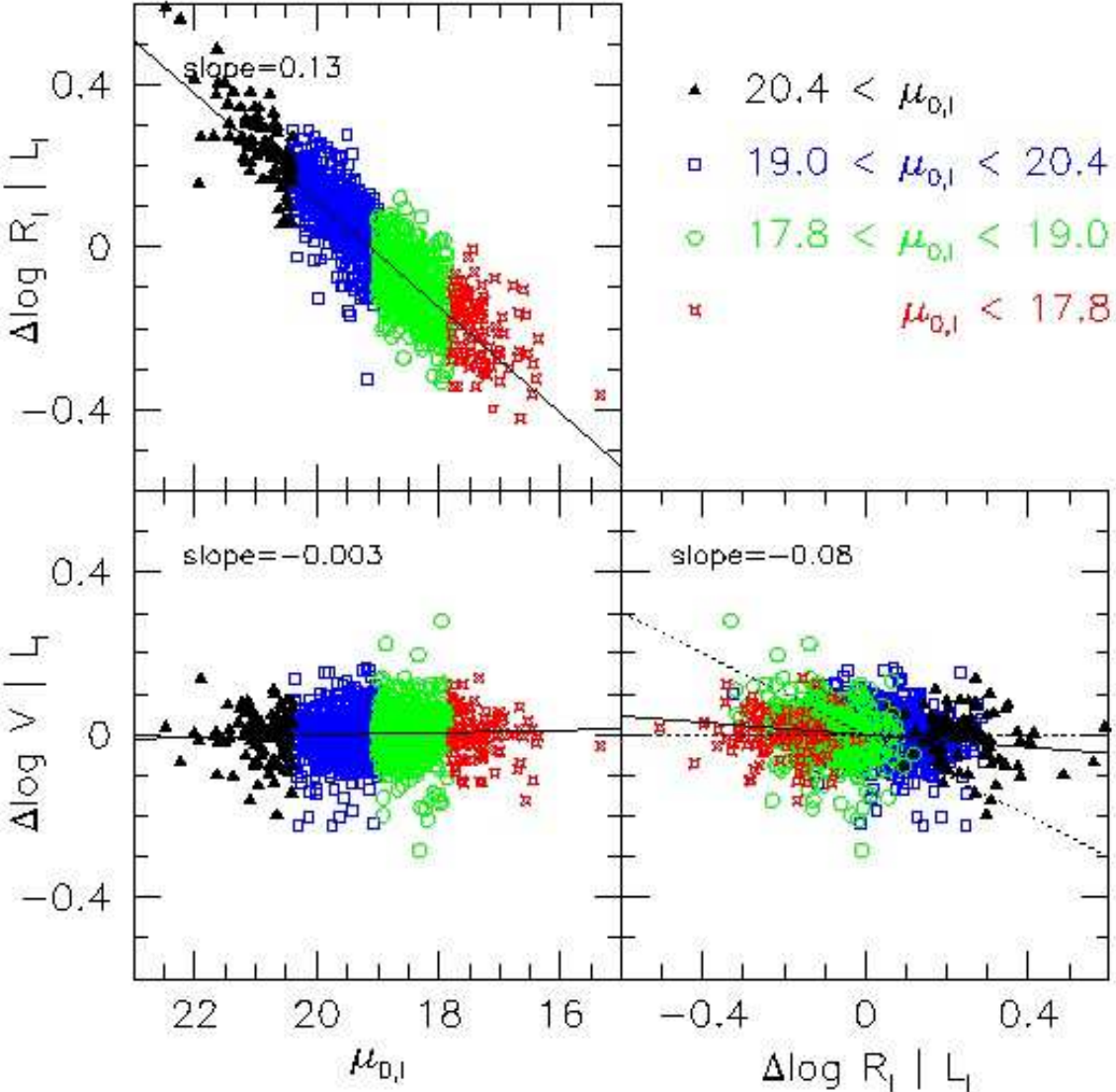


FIG. 2.— Residual correlations from the observed I-band *VLR* relations in Fig. 1. The black lines show weighted least-squares fits. The *RL* residuals show a clear correlation with surface brightness, while the *VL* residuals show none. The residuals of the *VL* and *RL* relation are only weakly correlated. The dotted line has a slope of -0.5 expected for a pure exponential disk (CR99).

with V_{CMB} the systemic velocity of the galaxy in the reference frame at rest with the cosmic microwave background (Kogut et al. 1993). The I -band luminosities are computed from M_I using an absolute magnitude for the Sun of $M_{I,\odot} = 4.19$.

Disk scale lengths are corrected for inclination using

$$R_I = R_{I,\text{obs}} / [1 + 0.4 \log(a/b)], \quad (6)$$

(Giovanelli et al. 1994), and converted into kilo parsecs using the angular diameter distance $D_A = V_{\text{CMB}} / [100h(1+z)]$.

Finally, central surface brightnesses are corrected for inclination, Galactic extinction, and cosmological dimming (*per unit frequency interval*) using

$$\mu_{0,I} = \mu_{0,I,\text{obs}} + 0.5 \log(a/b) - A_{\text{ext}} - 2.5 \log(1+z)^3. \quad (7)$$

The factor of 0.5 in front of the $\log(a/b)$ term is empirically determined by demanding that the residuals of the relation between central surface brightness and rotation velocity has no

inclination dependence¹. Following Giovanelli et al. (1997) we assume an uncertainty of 15% in γ_I , a/b , A_{ext} , and A_k , and propagate the errors. Not including distance uncertainties, the average errors on the observables are $\sigma_{\ln V} \simeq 0.08$, $\sigma_{\ln L} \simeq 0.1$, and $\sigma_{\ln R} \simeq 0.14$.

2.2. Scaling Relations

We now use the data described above to investigate the *VL* and *RL* relations of disk galaxies. Despite the fact that our sample consists of subsamples that use slightly different techniques or definitions for the scale lengths and rotation velocities, we find that, with the uniform inclination and extinction corrections described above, each subsample yields *VL* and *RL* relations that are consistent with each other (see Courteau et al. 2006 for details). We therefore combine the three subsamples to a single sample of ~ 1300 galaxies.

¹ For a disk of zero thickness one expects the factor to be between 0, for an optically thick disk, and 2.5, for an optically thin disk.

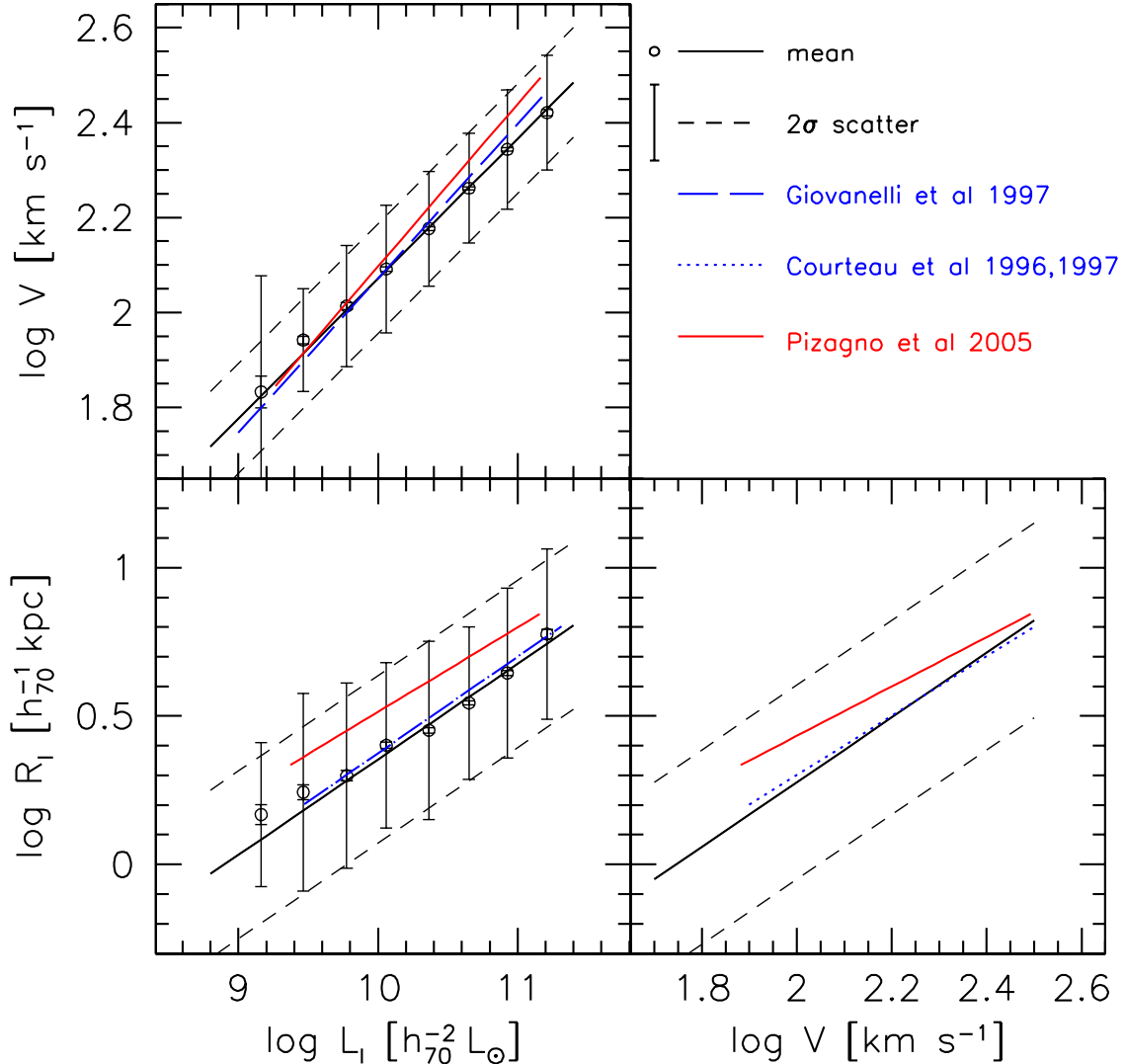


FIG. 3.— Comparison of our I-band VLR scaling relations with those from the literature. The long-dashed lines show the VL relation from Giovanelli et al. 1997 (G97), and the dotted lines show the RV relation from Courteau (1996, 1997). The red lines are derived from Pizagno et al. (2005).

The resulting VLR relations are shown in Fig. 1. The solid lines show the mean relations, which have been determined using bi-weighted orthogonal least-squares fits. The dashed lines show the 2σ scatter. The open circles with error bars show the data mean and 2σ scatter in separate luminosity bins with a width of 0.3 dex. These show that the VL and RL relations are well fitted with a single power-law over the range considered here. The RV relation has the largest scatter, and is thus the least well determined. For consistency we use the mean VL and RL relations to determine the mean RV relation.

The mean relations thus derived are:

$$\log \frac{V}{[\text{km s}^{-1}]} = 0.296 \log \frac{L_I}{[10^{10.3} h_70^{-2} L_\odot]} + 2.162, \quad (8)$$

$$\log \frac{R_I}{[h_70^{-1} \text{kpc}]} = 0.322 \log \frac{L_I}{[10^{10.3} h_70^{-2} L_\odot]} + 0.455. \quad (9)$$

$$\log \frac{R_I}{[h_70^{-1} \text{kpc}]} = 1.086 \log \frac{V}{[\text{km s}^{-1}]} - 1.894. \quad (10)$$

where R_I is the de-projected disk scale length in the photo-

metric I -band, and $h_{70} = H_0/(70 \text{ km s}^{-1} \text{ Mpc}^{-1})$.

The color coding in Fig. 1 denotes the central surface brightness of the disk in the I -band, $\mu_{0,I}$. Note that the scatter in the VL relation is not correlated with $\mu_{0,I}$. This is also apparent from Fig. 2 which shows the correlations between the residuals of the VL and RL relations at constant L ($\Delta \log V$ and $\Delta \log R$, respectively) and surface brightness, $\mu_{0,I}$. Again the symbols are color coded according to $\mu_{0,I}$. As is evident from the upper left panel, the scatter in the RL relation is by definition² dominated by scatter in surface brightness. The residuals of the VL relation, however, show no significant correlation with surface brightness at all (lower left panel). In addition, the VL and RL residuals are only very weakly correlated (lower right panel): the slope of the residual correlation is $\gamma \equiv d[\Delta \log V(L)]/d[\Delta \log R(L)] = -0.08 \pm 0.03$, in agreement with CR99.

² A family of pure exponential disks with constant Υ_I has, at a constant L_I , $\Delta \log R \propto 0.2 \mu_{0,I}$, which is different from the observed slope of 0.13. This owes to the relatively small range of luminosities sampled, relative to the amount of scatter in the RL relation.

Fig. 3 shows a comparison of the VLR relations derived here with previous studies. The black lines and point types are the same as in Fig. 1. The long-dashed and dotted lines show the VL relation from Giovanelli et al. (1997), and the RV relation that fits the data of Courteau (1996, 1997). Note that these VL and RL relations, which are in excellent agreement with our mean scaling relations, were used by MMW and FA00 as model constraints. The red lines in Fig. 3 show the VLR relations of Pizagno et al. (2005). The latter study is based on a sample of 81 disk dominated ($B/D < 0.11$) galaxies, with luminosities in the Sloan i -band, disk scale lengths measured with bulge-to-disk decompositions, and velocities measured at 2.2 disk scale lengths from $H\alpha$ rotation curves. We convert from L_i to L_I using $\log L_I = \log L_i + 0.4(i-I) - 0.4(i-I)_\odot \simeq 0.036$, assuming $M_{i,\odot} = 4.56$, and $(i-I) \simeq 0.46$ (Courteau et al. 2006). Note that the slope of the VL relation of Pizagno et al. (2005) is somewhat steeper than ours, while their RL relation is offset from ours towards larger disk scale lengths. These differences may be due to a combination of their relatively small sample size (81 galaxies), their bulge-to-disk ratio selection criteria, and different inclination corrections. These differences do not significant impact on our main conclusions, as we discuss in Appendix A

3. DISK FORMATION MODELS

In the standard picture of disk formation (e.g., Fall & Efstathiou 1980), disks form inside virialized dark matter halos through the cooling of the baryonic material. Our models are based on this standard picture, and closely follow MMW, but with some additional ingredients. In particular, we include a model for the formation of bulges, we use a prescription for star formation which separates the disk into gaseous and stellar components, we use an improved and generalized description for adiabatic contraction, and we use empirical relations to convert our models to observable quantities for direct comparison with the data described above. All these model ingredients are discussed in more detail below.

Although we refer to our models as ‘disk formation models’ they are completely ‘static’ (i.e., the model is not actually evolved). For a given specific angular momentum of the baryonic material out of which the disk forms and a given potential due to the dark matter, the structural properties of the resulting disk are computed assuming (i) that disks are exponential, and (ii) that the specific angular momentum of the baryonic material is conserved. Alternatively, one could in principle consider more ‘dynamic’ models, that follow the actual formation of the disk galaxies starting at high redshifts (e.g., Firmani & Avila-Reese 2000; Avila-Reese & Firmani 2000; van den Bosch 2001, 2002). However, as long as the formation of the disk is sufficiently quiescent, the final structure of the disk should be independent of its actual formation history: the structural properties of the final disk are basically just governed by the principle of dynamical, centrifugal equilibrium. In a more dynamic approach, one can actually model the star formation history of the disk, which is not possible with our static model. However, the star formation history mainly governs the final mass-to-light ratio of the stars, which we set using empirical relations. The models described here should thus be applicable independent of the detailed formation history as long as the two assumptions mentioned above are satisfied.

Unless stated otherwise we adopt a Λ CDM cosmology with $\Omega_m = 0.3$, $\Omega_b = 0.044$, $\Omega_\Lambda = 0.7$, $h = H_0/(100 \text{ km s}^{-1} \text{ Mpc}^{-1}) = 0.7$ and with a scale-invariant initial power spectrum with a

normalization $\sigma_8 = 0.9$. The baryonic mass fraction of this cosmology $f_{\text{bar}} \simeq 0.15$.

3.1. Disk Formation

We model dark matter halos as spheres with a NFW density distribution

$$\rho(r) = \frac{4\rho_s}{(r/r_s)(1+r/r_s)^2} \quad (11)$$

(Navarro, Frenk & White 1997) where r_s is a characteristic radius at which the logarithmic slope of the density distribution $d \ln \rho / d \ln r = -2$, and $\rho_s = \rho(r_s)$. The overall shape of the density distribution can be characterized by the so-called concentration parameter $c = R_{\text{vir}}/r_s$. Here R_{vir} is the virial radius, which is defined as the radius inside of which the average halo density is Δ_{vir} times the critical density for closure. For the Λ CDM cosmology adopted here $\Delta_{\text{vir}} \simeq 100$ (Bryan & Norman 1998). In addition to the virial radius R_{vir} we also define the virial velocity V_{vir} as the circular velocity at the virial radius, i.e., $V_{\text{vir}}^2 = GM_{\text{vir}}/R_{\text{vir}}$, with G the gravitational constant.

The total angular momentum of a halo, J_{vir} , is commonly expressed in terms of the dimensionless spin parameter:

$$\lambda = \frac{J_{\text{vir}}|E|^{1/2}}{GM_{\text{vir}}^{5/2}} = \frac{J_{\text{vir}}/M_{\text{vir}}}{\sqrt{2}R_{\text{vir}}V_{\text{vir}}} f_c^{1/2} \quad (12)$$

Here E is the halo’s energy, and f_c measures the deviation of E from that of a singular isothermal sphere with the same mass, and is given by

$$f_c = \frac{c}{2} \frac{1 - 1/(1+c)^2 - 2\ln(1+c)/(1+c)}{[c/(1+c) - \ln(1+c)]^2} \quad (13)$$

(see MMW).

We assume that the galaxy that forms consists of a bulge and a disk. Our algorithm to ascribe a bulge-to-disk ratio is discussed at the end of this section. We define the baryonic mass of the total galaxy as

$$M_{\text{gal}} \equiv M_{\text{d}} + M_{\text{b}} = m_{\text{gal}}M_{\text{vir}} \quad (14)$$

with M_{d} and M_{b} the masses of the disk and bulge, respectively, and $0 < m_{\text{gal}} \lesssim f_{\text{bar}}$. We define the bulge-to-disk mass ratio as $\Theta \equiv M_{\text{b}}/M_{\text{d}}$ so that

$$M_{\text{d}} = \frac{1}{1+\Theta} m_{\text{gal}}M_{\text{vir}} \quad (15)$$

$$M_{\text{b}} = \frac{\Theta}{1+\Theta} m_{\text{gal}}M_{\text{vir}}. \quad (16)$$

In addition, we write that the total angular momentum of the baryons out of which the disk plus bulge form is

$$J_{\text{gal}} \equiv j_{\text{gal}}J_{\text{vir}}. \quad (17)$$

As shown by van den Bosch et al. (2002), the specific angular momentum distribution of the total baryonic mass (including those baryons in the halo that do not partake in the formation of the disk plus bulge) is virtually identical to that of the dark matter. Therefore, one also expects that $0 < j_{\text{gal}} \lesssim f_{\text{bar}}$.

As discussed below, we assume that the bulge forms out of disk instabilities. Let $J_{\text{b}} = j_{\text{b}}J_{\text{vir}}$ indicate the original angular momentum of the baryonic material out of which the bulge forms. We assume, however, that the bulge formation process transfers this angular momentum to the disk plus the halo, so that the final angular momentum of the bulge is zero. Indeed,

such an angular momentum transfer is observed in numerical simulations (e.g., Hohl 1971; Debattista et al. 2006). If we define f_t as the fraction of J_b that is transferred to the disk, we obtain that the final angular momentum of the disk is equal to

$$J_d = [j_{\text{gal}} - (1 - f_t)j_b] J_{\text{vir}} \quad (18)$$

The *specific* angular momentum of the final disk is therefore

$$\frac{J_d}{M_d} = (1 + \Theta)[1 - f_{\text{lost}}] \left(\frac{j_{\text{gal}}}{m_{\text{gal}}} \right) \frac{J_{\text{vir}}}{M_{\text{vir}}} \quad (19)$$

where we have introduced the parameter

$$f_{\text{lost}} = (1 - f_t) \left(\frac{j_b}{j_{\text{gal}}} \right) \quad (20)$$

which expresses the fraction of the total angular momentum of the material out of which the bulge plus disk forms that has been lost to the halo. For modeling purposes it is more useful to define the parameter

$$f_x \equiv f_{\text{lost}} \left(\frac{1 + \Theta}{\Theta} \right) = (1 - f_t) \left(\frac{J_b/M_b}{J_{\text{gal}}/M_{\text{gal}}} \right) \quad (21)$$

which expresses the ratio of the *specific* angular momentum that has been lost to the halo due to bulge formation to the total *specific* angular momentum of the material out of which the disk plus bulge have formed. For example, $f_x = 1$ means that bulge formation does not change the specific angular momentum of the disk. The extreme $f_x = 0$ occurs when the disk loses mass but not angular momentum during bulge formation. Note that unlike f_{lost} , the parameter f_x can in principle be larger than unity. In practice, however, the bulge is likely to form out of material with relatively low specific angular momentum (e.g., Norman, Sellwood & Hassan 1996; van den Bosch et al. 2002). Furthermore, the fraction of angular momentum that is lost to the halo is expected to be fairly small (e.g., Weinberg 1985; Debattista & Sellwood 2000; Valenzuela & Klypin 2003; O'Neill & Dubinski 2003), so that f_t is expected to be close to unity.

For a disk with a surface density $\Sigma(R)$ and a circular velocity $V(R)$ the total angular momentum is

$$J_d = 2\pi \int_0^{R_{\text{vir}}} \Sigma(R) R V(R) R dR. \quad (22)$$

Throughout we assume that the disk that forms has an exponential surface density distribution $\Sigma(R) = \Sigma_0 \exp(-R/R_d)$, so that

$$J_d = 2M_d R_d V_{\text{vir}} f_v \quad (23)$$

with

$$f_v = \frac{1}{2} \int_0^{R_{\text{vir}}/R_d} e^{-u} u^2 \frac{V(uR_d)}{V_{\text{vir}}} du \quad (24)$$

(cf., MMW). If we combine equations (12), (19), and (23) we obtain the following expression for the scale length of the disk:

$$R_d = \frac{1}{f_v \sqrt{2f_c}} [1 + (1 - f_x)\Theta] \lambda_{\text{gal}} R_{\text{vir}} \quad (25)$$

where we have defined λ_{gal} as the effective spin parameter of the material out of which the bulge plus disk form:

$$\lambda_{\text{gal}} \equiv \left(\frac{j_{\text{gal}}}{m_{\text{gal}}} \right) \lambda \quad (26)$$

From equation (25) it is evident that bulge formation impacts the final scale length of the disk. Typically, for $f_x > 1$ the disk size will decrease, while $f_x < 1$ causes an increase in R_d . Note that the transition does not occur exactly at $f_x = 1$, because the presence of a bulge component modifies f_v . Numerical simulations indicate that bulge formation causes an increase in disk scale lengths (Debattista et al. 2006), suggesting that $f_x < 1$. Shen et al. (2003) considered a fairly similar model but with the assumption that the material that forms the bulge has the same specific angular momentum as the disk. Their favored model is equivalent to our model with $f_x = 0.5$. However, given the arguments above, we expect f_x to be smaller than this. In what follows we adopt a fiducial value of $f_x = 0.25$, although none of our results are very sensitive to this particular choice.

Note that since the computation of f_v requires knowledge of R_d , this set of equations has to be solved iteratively (see MMW for details). When computing the total circular velocity $V(R)$ we use that

$$V^2(R) = V_d^2(R) + V_b^2(R) + V_{\text{DM}}^2(R) \quad (27)$$

Here

$$V_d^2(R) = \frac{GM_d}{R_d} 2y^2 [I_0(y)K_0(y) - I_1(y)K_1(y)] \quad (28)$$

with $y = R/(2R_d)$, and I_n and K_n are modified Bessel functions (Freeman 1970). The circular velocities of the bulge, V_b , and the dark matter halo, V_{DM} , are computed assuming spherical symmetry, whereby the mass distribution of the dark matter halo is adjusted for adiabatic contraction (see §3.2 below). The density distribution of the bulge is assumed to follow a Hernquist (1990) profile

$$\rho_b = \frac{M_b}{2\pi} \frac{r_b}{r(r+r_b)^3} \quad (29)$$

In projection, this is similar to a de Vaucouleurs profile (i.e., a Sersic profile with Sersic index $n = 4$), with a half light radius, $R_{\text{eff}} = 1.8152r_b$ (Hernquist 1990). Throughout we adopt the relation between R_{eff} and M_b from Shen et al. (2003):

$$\log R_{\text{eff}} = \begin{cases} -5.54 + 0.56 \log M_b & (\log M_b > 10.3) \\ -1.21 + 0.14 \log M_b & (\log M_b \leq 10.3) \end{cases} \quad (30)$$

Although bulges of late-type disk galaxies are better described by exponential profiles (e.g. Courteau, de Jong & Broeils 1996), what matters most for our purposes is the *total* bulge mass; its distribution is only of secondary importance.

The computation of the actual bulge-to-disk ratio for each model galaxy is based on the fact that self-gravitating disks are unstable against global instabilities (e.g., bar formation). We follow the approach of van den Bosch (1998, 2000) and Avila-Reese & Firmani (2000) and assume that an unstable disk transforms part of its disk material into a bulge component in a self-regulating fashion, such that the final disk is marginally stable. Bars, which are considered the transitions objects in this scenario, are thus expected to be fairly common, as observed.

We define $\beta(R) = V_d(R)/V(R)$, and consider the disk to be stable as long as

$$\beta_{\text{max}} = \max_{0 \leq R \leq R_{\text{vir}}} \beta(R) < \beta_{\text{crit}} \quad (31)$$

(Christodoulou, Shlosman & Tohline 1995). The actual value of β_{crit} depends on the gas mass fraction of the disk, but falls

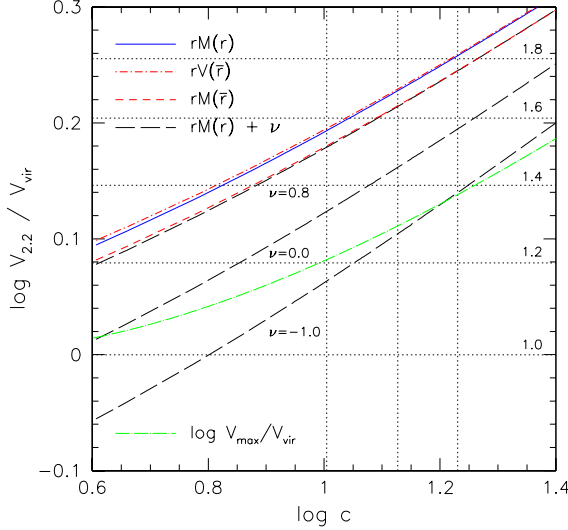


FIG. 4.— Ratio of observed to virial circular velocities, $V_{2,2}/V_{\text{vir}}$, as a function of the concentration parameter, for various forms of adiabatic contraction. All models have $\lambda_{\text{gal}} = 0.048$ and $m_{\text{gal}} = 0.05$. The vertical dotted lines show the mean c according to model of Bullock et al. (2001a) for halos with virial mass, $M_{\text{vir}} = 10^{13}, 10^{12}, \& 10^{11} h^{-1} M_{\odot}$. The horizontal dotted lines show $V_{2,2}/V_{\text{vir}}$ ratios of 1 to 1.8 at intervals of 0.2. The relation using the standard (Blumenthal et al. 1986) adiabatic invariant, $rM(r)$, is given by the blue solid line. The modified adiabatic invariant, $rM(\bar{r})$, as proposed by Gnedin et al. 2004 results in only a $\simeq 0.02$ dex ($\simeq 5\%$) reduction in $V_{2,2}$ (red short dashed line). Most of this reduction is taken back if we use specific angular momentum as the adiabatic invariant, and take into account the disk geometry when computing V_{circ} (dot-dashed red line). For all of these adiabatic contraction models, standard concentration parameters yield $V_{2,2}/V_{\text{vir}} \simeq 1.6$. The black long-dashed lines show models where we have artificially modified the contraction factor (see equation 34). Starting from the standard model ($\nu = 1$), the $rM(\bar{r})$ relation is approximately reproduced with $\nu = 0.8$, $\nu = 0$ results in no adiabatic contraction of the halo, while $\nu = -1$ gives halo expansion. The green dot-long dashed line shows $V_{\text{max}}/V_{\text{vir}}$, where V_{max} is the maximum halo circular velocity (without adiabatic contraction).

roughly in the range $0.52 \lesssim \beta_{\text{crit}} \lesssim 0.70$. For a given value of β_{crit} , we use an iterative technique to find the bulge-to-disk ratio for which $\beta_{\text{max}} = \beta_{\text{crit}}$.

3.2. Adiabatic Contraction

When baryons cool and concentrate in the center of a dark matter halo they deepen and modify the shape of the gravitational potential. If this process is slow with respect to the (local) dynamical time of the halo, the halo will contract to conserve its adiabatic invariants. For the idealized case of a spherical halo in which all dark matter particles move on circular orbits, the adiabatic invariants reduce to the specific angular momentum, $rV(r)$. If, in addition, the distribution of the baryons has spherical symmetry, this reduces further to $rM(r)$, with $M(r)$ the enclosed mass within radius r (Blumenthal et al. 1986; hereafter BFFP).

In realistic dark matter halos, however, the particles typically move on highly eccentric orbits (Ghigna et al. 1998; van den Bosch et al. 1999). Taking this into account reduces the effect of adiabatic contraction (Wilson 2003). Gnedin et al. (2004) give a modified adiabatic invariant, $rM(\bar{r})$, where $\bar{r} \simeq 0.85(r/R_{\text{vir}})^{0.8}$ is the orbit averaged radius. Using this adiabatic invariant results in somewhat less contraction of the halo than in the standard BFFP formalism. An additional problem is that disks are not spherical. Therefore, in principle one should use $rV(r)$ as the adiabatic invariant, rather than $rM(r)$. It is well known that the circular velocity curve of

a thin exponential disk rises less rapidly but reaches a higher peak velocity than a sphere with the same enclosed mass (e.g., Binney & Tremaine 1987). Therefore, using $rV(r)$ as an adiabatic invariant, rather than $rM(r)$, results in a stronger contraction of the dark matter halo at 2.2 disk scale lengths.

In addition to these somewhat subtle problems for the standard BFFP formalism, one may also question whether adiabatic contraction really occurs during disk formation. If disks are not built by smooth, relatively slow, spherical infall, the adiabatic contraction could, in principle, be counter-balanced by a variety of processes. These may even go as far as to cause an actual expansion of the dark matter distribution. One such process is dynamical friction (e.g. El-Zant, Shlosman & Hoffman 2001; Ma & Boylan-Kolchin 2004; Mo & Mao 2004; Tonini, Lapi & Salucci 2006), which could be significant if disks are built by relatively big clumps. Indeed, the physics of gas cooling suggests that disks may have formed out of clumpy, cold streams rather than from a smooth cooling flow (Birnboim & Dekel 2003; Maller & Bullock 2004; Dekel & Birnboim 2006; Kaufmann et al. 2006; Keres et al. 2005). We defer a detailed study of the effects of such cold infall on the contraction of the halo to a future paper. Here we consider a simple modification of the BFFP adiabatic contraction formalism that allows us, with a single tunable parameter, to consider reduced contraction, no contraction, or even expansion.

Our method starts from the BFFP formalism, according to which a dark matter particle initially (i.e., before the formation of the disk plus bulge) at radius r_i settles at a radius r_f , where

$$r_f M_f(r_f) = r_i M_i(r_i). \quad (32)$$

Here $M_i(r)$ and $M_f(r)$ are the initial and final mass distributions. If we assume that initially the baryons have the same (normalized) density distribution as the dark matter, then $M_i(r)$ is simply given by the initial halo profile (e.g. NFW). For the final mass distribution we have that

$$\begin{aligned} M_f(r_f) &= M_d(r_f) + M_b(r_f) + M_{\text{DM},f}(r_f) \\ &= M_d(r_f) + M_b(r_f) + (1 - m_{\text{gal}}) M_i(r_i) \end{aligned} \quad (33)$$

Here $M_d(r)$ is the mass of the exponential disk enclosed within spherical shells of radius r , $M_b(r)$ is the similarly enclosed mass of the Hernquist bulge, and the second equality follows from the assumption that adiabatic contraction occurs without shell crossing. Equations (32) and (33) can be solved iteratively for the contraction factor $\Gamma(r_i) \equiv r_f/r_i$, which then allows for a computation of the mass distribution of the contracted dark matter halo.

Our modification consists of simply defining the *actual* relation between r_f and r_i as

$$r_f = \Gamma^\nu r_i \quad (34)$$

with ν a free parameter: $\nu = 1$ yields the standard BFFP contraction, $\nu = 0$ corresponds to no adiabatic contraction, and $\nu < 0$ models an expansion of the dark matter halo. As a specific example of an expansion model, $\nu = -1$ results in an expansion factor that is equal to the contraction factor in the BFFP model.

Fig. 4 shows the impact of various adiabatic contraction formalisms on the ratio of the total circular velocity at 2.2 disk scale lengths, $V_{2,2}$, to the virial velocity, V_{vir} . We consider models with an effective spin parameter $\lambda_{\text{gal}} = 0.048$ and a baryonic mass fraction $m_{\text{gal}} = 0.05$ (no bulge formation is considered here). We apply the various contrac-

tion formalisms described above and compute the resulting $V_{2.2}/V_{\text{vir}}$ as a function of the halo concentration parameter c . The three vertical dashed lines (from left to right) indicate the mean halo concentration expected for halos of mass $M_{\text{vir}} = 10^{13}, 10^{12}, \text{ & } 10^{11} h^{-1} M_{\odot}$ in the model of Bullock et al. (2001a).

Note that with the standard BFFP adiabatic contraction ($\nu = 1$), and a mean halo concentration parameter for a halo of mass $M_{\text{vir}} = 10^{12} h^{-1} M_{\odot}$, we expect that $V_{2.2}/V_{\text{vir}} \simeq 1.7$, while $V_{2.2}/V_{\text{vir}} \simeq 1.45$ without adiabatic contraction ($\nu = 0$). In the extreme case where the halo is adiabatically expanded ($\nu = -1$) the ratio is further lowered to $V_{2.2}/V_{\text{vir}} \simeq 1.3$. As an illustration we also plot $V_{\text{max}}/V_{\text{vir}}$, where V_{max} is the maximum circular velocity of a NFW halo, which is related to the halo concentration as

$$\frac{V_{\text{max}}}{V_{\text{vir}}} \sim 0.465 \sqrt{\frac{c}{\ln(1+c) - c/(1+c)}}. \quad (35)$$

Note that for the typical concentration of galaxy sized halos $V_{2.2} \simeq V_{\text{max}}$ if $\nu \simeq -1$.

The short dashed (red) line in Fig. 4 shows the results for the adiabatic invariant $rM(\bar{r})$ proposed by Gnedin et al. (2004). As mentioned above, this adiabatic invariant results in a somewhat smaller overall contraction than the standard BFFP formalism. Note that we can accurately model the Gnedin et al. formalism by simply setting $\nu = 0.8$. Not only does this reproduce $V_{2.2}$ but also the *shape* of the circular velocity profile. Finally, the dot-short dashed (red) line shows the results for the adiabatic invariant $rV(\bar{r})$, with \bar{r} the orbit averaged radius of Gnedin et al. (2004). This adiabatic invariant accounts for both the eccentricity of the orbits of the dark matter particles and for the (non-spherical) geometry of the disk. Note that the resulting $V_{2.2}/V_{\text{vir}}$ is virtually indistinguishable from what one obtains with the standard BFFP formalism: taking account of the non-sphericity of the disk completely cancels the impact of non-circular orbits.

3.3. Star Formation

Disks are made up of stars and cold gas. In the highest surface brightness galaxies the gas fraction (defined as the ratio of cold gas mass to total disk mass) is small, typically $\sim 10\%$, so assuming a pure stellar disk is reasonable. However, the gas fraction increases with decreasing surface brightness and luminosity (McGaugh & de Blok 1997; Kannappan 2004) such that low surface brightness galaxies have comparable amounts of mass in cold gas and stars. The data used here, however, only provides measurements of the stellar disks, while the models describe the distribution of total baryonic matter (cold gas plus stars). To allow for a proper comparison between models and data we need a prescription for computing the ratio between stars and cold gas as function of radius in the galaxy.

Kennicutt (1989) has shown that star formation is strongly suppressed below a critical surface density, which can be modeled by a simple Toomre stability criterion:

$$\Sigma_{\text{crit}}(R) = \frac{\sigma_{\text{gas}} \kappa(R)}{3.36 Q G} \quad (36)$$

(Toomre 1964). Here $\kappa(R) = \sqrt{2} \frac{V(R)}{R} (1 + \frac{d \ln V(R)}{d \ln R})^{\frac{1}{2}}$ is the epicycle frequency, σ_{gas} is the velocity dispersion of the gas, and Q is the Toomre stability parameter. Throughout we adopt $\sigma_{\text{gas}} = 6 \text{ km s}^{-1}$ and $Q = 1.5$; with this choice of parameters the

radius at which star formation is observed to truncate coincides with the radius where $\Sigma_{\text{gas}} = \Sigma_{\text{crit}}$ (Kennicutt 1989).

We compute the total stellar mass as

$$M_* = M_b + 2\pi \int_0^{R_{\text{SF}}} [\Sigma(R) - \Sigma_{\text{crit}}(R)] R dR \quad (37)$$

where R_{SF} is the star formation truncation radius, defined by $\Sigma(R_{\text{SF}}) = \Sigma_{\text{crit}}(R_{\text{SF}})$. Note that we thus assume that the bulge is made of stars entirely, and that all the disk material with a surface density above the critical density has been converted into stars. Although this is clearly an over-simplification of the complicated physics associated with star formation, there are several reasons why this is probably reasonable. Firstly, it is a clear improvement over the assumption that disks consist of stars only, such as in the standard MMW model. Secondly, as shown by van den Bosch (2000, 2001), this simple model (i) matches the gas mass fractions of disk galaxies as function of their surface brightness and luminosity, and (ii) naturally leads to gas disks that are more extended than stellar disks. Finally, more detailed, ‘dynamic’ models for disk formation, which model the actual star formation rate using realistic, empirically motivated, prescriptions, show that the typical star formation time scale is short compared to the time scale on which the disk accretes new gas. Consequently, these models indeed predict that the gas disk has been depleted by star formation down to $\Sigma_{\text{gas}} = \Sigma_{\text{crit}}$ (van den Bosch 2001). As we will see later, the inclusion of a star formation threshold density proves a crucial ingredient in solving two problems of the standard MMW model.

3.4. Conversion from Mass to Light

In order to compare our models with observations, we need to convert both the stellar masses and the stellar disk scale lengths into the observed *I*-band luminosities and scale lengths, respectively.

The conversion from mass to light is conventionally done via the mass-to-light ratio, $\Upsilon \equiv M_*/L$. Bell & de Jong (2001) showed that Υ can be estimated from optical colors. These relations have been updated by Bell et al. (2003a) and Portinari, Sommer-Larsen & Tantalo (2004). The main uncertainty in this method is the normalization, reflecting the unknown stellar IMF. Additional uncertainties arise from details related to the amount of dust extinction and the star formation histories. Upper limits on the normalization can be obtained from maximal disk fits to observed rotation curves, as shown in Bell & de Jong (2001), although these may still suffer from distance uncertainties. More accurate estimates from rotation curve mass modeling are hindered by well known degeneracies (e.g., van Albada et al. 1985; van den Bosch et al. 2000; Dutton et al. 2005).

For the sub-sample of our galaxies with optical colors, we apply the relations in Bell et al. (2003a), to obtain estimates of Υ_I . These are based on a ‘dust’-Salpeter IMF, introduced by (Bell & de Jong 2001). We have verified that, assuming the same IMF, the relations of Portinari et al. (2004) give very similar results that agree to within 0.05 dex. In Fig. 5 we plot the resulting Υ_I as a function of the *I*-band luminosity. The solid red line shows the bi-weighted orthogonal least squares fit to these points, and is given by

$$\log \frac{\Upsilon_I}{[M_{\odot}/L_{\odot}]} = 0.172 + 0.144 \log \frac{L_I}{[10^{10.3} h_{70}^{-2} L_{\odot}]} + \Delta_{\text{IMF}}, \quad (38)$$

The intrinsic scatter in this relation is estimated to be $\simeq 0.1$ dex (Bell et al. 2003a, Kauffmann et al. 2003a). We model this scatter by drawing Υ_I for each model disk galaxy from a log-normal distribution with a mean given by eq. (38) and with a scatter $\sigma_{\ln \Upsilon_I}$, which we treat as a free parameter. The other free parameter, Δ_{IMF} , absorbs our lack of knowledge about the IMF. It is equal to zero for the ‘diet’-Salpeter IMF assumed here, while $\Delta_{\text{IMF}} \simeq +0.15$ for a Salpeter (1955) IMF, and $\Delta_{\text{IMF}} \simeq -0.15$ for a top-heavy IMF like that of Kennicutt (1983). See Portinari et al. (2004) for details.

As a consistency check, we apply the Bell et al. (2003a) relations to the mean $(g-r)$ color-luminosity relation of Pizagno et al. (2005). The resulting $\Upsilon_I(L_I)$ is indicated as the long dashed line in Fig. 5 and agrees with our mean relation to within 0.05 dex. For comparison, we also show the Υ_I adopted by previous studies. The short-dashed line shows the relation adopted by FA00; the relatively weak slope of their $\Upsilon_I(L_I)$ relation was derived from a comparison of the slopes of I -band and H -band Tully-Fisher relations, while their normalization is based on the somewhat ad hoc assumption that the disk contributes 70 percent to the circular velocity at 2.2 disk scale lengths. Finally, McGaugh et al. (2000) and MMW both adopted a constant mass-to-light ratio (independent of luminosity). The value adopted by McGaugh et al. (2000), $\Upsilon_I = 1.7(M/L_I)_\odot$, is based on a stellar population synthesis model with a Salpeter IMF, while MMW based their value, $\Upsilon_I = 1.7h(M/L_I)_\odot$ on the sub-maximal disk arguments of Bottema (1993). Note, however, that there is an error in MMW, and that the actual value they used is $\Upsilon_I = 1.19h(M/L_I)_\odot$ (H.J. Mo 2004, *private communication*). Note that this value is small compared to the typical mass-to-light ratios shown here. As we will demonstrate below, this has important implications for the MMW results.

3.4.1. Disk Scale Lengths

In order to compute the I -band scale lengths of our model disks, for direct comparison with the data discussed in §2, we proceed as follows.

For each galaxy we first compute the stellar surface density profile of the disk, i.e., $\Sigma_* = \Sigma(R) - \Sigma_{\text{crit}}(R)$ with $0 \leq R \leq R_{\text{SF}}$, which we fit with an exponential disk over the radial range $0.15R_{\text{SF}} \leq R \leq 0.80R_{\text{SF}}$.

In theoretical models of disk galaxy formation, disks form inside out. This results in color gradients, with progressively larger scale lengths when going from stellar mass to K -band light (assumed to closely trace the underlying stellar mass) to B -band light. Observations show a similar trend with $R_R/R_H = 1.17$ (MacArthur, Courteau, & Holtzman 2003), and $R_I/R_K = 1.13$ (de Jong 1996), where subscripts denote the photometric band. To account for these color gradients we convert our stellar disk scale lengths to I -band scale lengths using $\log R_I = \log R_* + 0.05$, with R_* the scale length of the exponential fit to the model stellar disk. Note that this assumes the scale length in stellar mass, R_* , is equal to the scale length in K -band light, R_K , and thus is probably an underestimate of the true correction.

3.5. Sampling Strategy

In order to pursue a meaningful comparison of our model VL and RL relations with the observations, we construct samples of random realizations of model galaxies. Each model galaxy is specified by four parameters; the virial mass of the halo, M_{vir} , the halo concentration parameter, c , the effective

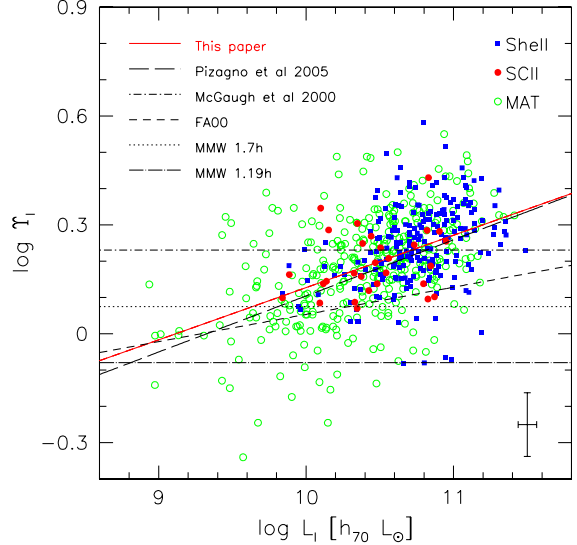


FIG. 5.— I-band stellar mass-to-light ratio, Υ_I , versus I-band luminosity. The points show Υ_I estimated from optical colors using the relations in Bell et al. (2003a). These data form a sub-sample of the Courteau et al. (2006) data set: MAT (green), Shell (blue), and SCII (red). A typical 1σ error bar is given in the lower right corner. The solid red line gives the bi-weighted fit to these data. As a consistency check the long dashed line gives the relation computed using the mean $(g-r)$ color-luminosity relation from Pizagno et al. (2005) and the Υ_I - $(g-r)$ color relation from Bell et al. (2003a). We transform i -band luminosities into I -band luminosities with $L_I = L_i - 0.036$ (Courteau et al. 2006). This relation is in excellent agreement with ours. For comparison we give the $\Upsilon_I = 1.7$ estimate of McGaugh et al. (2000; dot-dashed line), $\Upsilon_I(L_I)$ relation from FA00 (short-dashed line), and the adopted $\Upsilon_I = 1.7h$ (dotted line) and the used $\Upsilon_I = 1.19h$ (dot-long dashed line) by MMW.

spin parameter of the galaxy, λ_{gal} , and the baryonic mass fraction of the galaxy, m_{gal} .

Previous studies (e.g., MMW; Somerville & Primack 1999; Cole et al. 2000; van den Bosch 2000; Firmani & Avila-Reese 2000; Croton et al. 2006) have assumed that $\lambda_{\text{gal}} = \lambda$. However, there are numerous reasons why the spin parameter of the disk may be different from that of its dark matter halo (see §5). In this paper we assume that λ_{gal} follows a log-normal distribution:

$$p(\lambda_{\text{gal}}) d\lambda_{\text{gal}} = \frac{1}{\sigma_{\ln \lambda} \sqrt{2\pi}} \exp \left[-\frac{\ln^2(\lambda_{\text{gal}}/\bar{\lambda}_{\text{gal}})}{2\sigma_{\ln \lambda}^2} \right] \frac{d\lambda_{\text{gal}}}{\lambda_{\text{gal}}}, \quad (39)$$

and we treat $\bar{\lambda}_{\text{gal}}$ and $\sigma_{\ln \lambda}$ as free parameters. If $\lambda_{\text{gal}} \simeq \lambda$ we expect that $\bar{\lambda}_{\text{gal}} \simeq 0.042$ and $\sigma_{\ln \lambda} \simeq 0.5$, which are the values obtained for dark matter haloes from cosmological numerical simulations (Bullock et al. 2001b). In what follows we will consider these as our fiducial values.

The concentration parameter, c , is strongly correlated with the halo mass accretion history (Wechsler et al. 2002; Zhao et al. 2003; Li, Mo & van den Bosch 2005), and thus depends on both halo mass and cosmology. Bullock et al. (2001a) and Eke, Navarro, & Steinmetz (2001) present analytical models, calibrated against numerical simulations, for the computation of a mean concentration given a halo mass and cosmology. In what follows we use the model by Bullock et al. (2001a). At a given halo mass, the halo concentrations follow a log-normal distribution with a scatter $\sigma_{\ln c} = 0.32$ (Wechsler et al. 2002). However, as for the spin parameter, the mean and scatter are different for the subset of halos without a recent major merger. As shown by Wechsler et al. (2002), the scatter becomes

TABLE 1
OVERVIEW OF MODEL PARAMETERS AND THEIR FIDUCIAL
VALUES

Parameter	symbol	fiducial value
Median effective spin parameter	$\bar{\lambda}_{\text{gal}}$	0.042
Concentration parameter normalization	η_c	1.0
Adiabatic contraction parameter	ν	1.0
Toomre stability parameter	Q	1.5
Bulge formation threshold	β_{crit}	1.0
Bulge formation exchange parameter	f_x	0.5
Galaxy mass fraction normalization	$m_{\text{gal},0}$	0.05
Galaxy mass fraction slope	α_m	0.0
Mass-to-light ratio normalization	Δ_{IMF}	0.0

smaller while the mean increases. To be able to account for this, we consider $\sigma_{\ln c}$ a free parameter and compute $c(M_{\text{vir}})$ using the relation by Bullock et al. (2001a) but multiplied by a free parameter η_c .

Unlike for c and λ , very little is known regarding the baryonic mass fractions, m_{gal} , of galaxies. We account for this limitation by modeling the mean as

$$\bar{m}_{\text{gal}}(M_{\text{vir}}) = m_{\text{gal},0} \left(\frac{M_{\text{vir}}}{10^{11.5} h^{-1} M_{\odot}} \right)^{\alpha_m} \quad (40)$$

with $m_{\text{gal},0}$ and α_m two free parameters. The value of α_m is related to the relative efficiencies of cooling and feedback processes. Typically, cooling results in $\alpha_m < 0$ while feedback results in $\alpha_m > 0$ (e.g., Dekel & Silk 1986; van den Bosch 2002). Finally, to allow for scatter in the above relation, we assume that, at fixed halo mass, m_{gal} follows a log-normal distribution with scatter $\sigma_{\ln m}$, which we also consider a free parameter.

To construct *VL* and *RL* relations for our models we proceed as follows. We uniformly sample a range in $\log M_{\text{vir}}$. For each halo, we then draw values for c , λ_{gal} , and m_{gal} using the log-normal distributions described above. We then iterate until a solution for the disk-to-bulge ratio is found, taking adiabatic contraction into account, and compute the resulting galaxy luminosity, L_I , disk scale length R_I , (both in the *I*-band), as well as the circular velocity, $V_{2,2}$, of the model galaxy at $2.2R_I$. To mimic the observational errors we add to each of the three model observables $\log V_{2,2}$, $\log L_I$, and $\log R_I$ a Gaussian deviate with a dispersion that reflects the typical observational errors. The uniform sampling of halos in $\log M_{\text{vir}}$ results in approximately uniform sampling in $\log L_I$, while the luminosity sampling of the data is approximately log-normal with a low luminosity tail. To allow for a fair comparison with the data we need to reproduce the observed luminosity sampling. We do this with a Monte-Carlo technique which accepts model galaxies such that they reproduce the observed luminosity distribution. Finally, when including bulge formation, we tune β_{crit} so as to roughly reproduce the observed distribution of bulge-to-disk ratios of our data sample.

3.6. Overview of Model Parameters

A list of the free model parameters with their fiducial values is given in Table 1. The fiducial value $\beta_{\text{crit}} = 1.0$ corresponds to a model without bulge formation.

In addition to these model parameters, there are four parameters that describe the amounts of scatter in the log-normal distributions of c , λ_{gal} , m_{gal} and Υ_I , and which we also treat as free parameters in what follows.

4. COMPARISON BETWEEN MODELS AND DATA

In order to gain some insight into the origin of the slopes and zero-points of the *VL* and *RL* relations, we start by considering a set of simplified models without bulge formation ($\beta_{\text{crit}} = 1.0$), and without scatter ($\sigma_{\ln c} = \sigma_{\ln \lambda} = \sigma_{\ln m} = \sigma_{\ln \Upsilon} = 0$). More complete models, including both bulge formation and scatter will be presented in §4.2.

4.1. Median Parameter Relations

4.1.1. Slopes

We start by reproducing the models of MMW. To this extent we set $\alpha_m = 0$, $Q = \infty$ (i.e., entire disk is made of stars), and $\Upsilon_I = 0.83$ (i.e. 1.19×0.7). As can be seen in the left-hand panels of Fig. 6 this model reproduces the slope of the *VL* relation, but predicts a somewhat steeper slope for the *RL* relation than observed. The deviations of the slopes of both the *VL* and *RL* relations from the virial value of $1/3$ are due to the non-homology of the dark matter halos (i.e., the $c(M_{\text{vir}})$ relation). Our deviations from the pure virial equations are somewhat larger than in MMW. This owes to the fact that we use the halo concentration model of Bullock et al. (2001a), which predicts a much stronger mass dependence than the NFW model used by MMW. The Bullock et al. (2001a) model also predicts higher c than the NFW model. This accounts for the slight discrepancy between the *VL* zero point of our model and the data.

Panels in the second column from the left show the same model, but with the more realistic $\Upsilon(L)$ relation of eq. (38). Note that the slopes of both the *VL* and *RL* relations are now significantly steeper than the data. In the third column of Fig. 6, we include the star formation threshold to separate the disk into stars and gas. Since lower luminosity galaxies have higher gas-to-stellar mass ratios this flattens the *VL* slope, bringing it back in agreement with the data³. The star formation threshold also results in smaller stellar disk scale lengths compared to the baryonic disk scale lengths. However, this reduction is approximately canceled out by the reduction in luminosity so that the *RL* slope and zero points are not significantly affected by the star formation threshold. Finally, in order to match the *RL* slope we tune α_m to match the slope of the *RL* relation. This requires $\alpha_m = 0.18$, so that the galaxy mass fraction, m_{gal} , increases with increasing halo mass, as expected, for example, for simple supernova feedback models (e.g., Dekel & Silk 1986; van den Bosch 2002; Dekel & Woo 2003). As shown in the right-hand panels of Fig. 6 this model roughly matches the slopes of both the *VL* and *RL* relations, and will hereafter serve as our reference model.

Although the introduction of a non-zero α_m causes the galaxy mass fractions, m_{gal} , to systematically vary by a factor ~ 3 over the luminosity range probed, this does not significantly impact the slope of the *VL* relation. This owes to the fact that variance in m_{gal} scatters galaxies mainly along the *VL* relation: an increase in m_{gal} makes the galaxy more luminous but simultaneously increases its rotation velocity (see also Navarro & Steinmetz 2000). This important aspect, which we discuss in more detail in §4.2 below, implies that we can simply tune α_m and $m_{\text{gal},0}$ to fit the slope and zero point of the *RL* relation, without (strongly) affecting the *VL* relation.

³ We emphasize that the luminosity dependence of the gas-to-stellar mass ratio is the key ingredient to this success, not the mechanism by which this is achieved. Therefore any argument against Σ_{crit} as a physical threshold for star formation is not relevant here. All that matters is that our separation of disk mass in stars and cold gas reproduces the gas-to-stellar mass ratios as a function of disk luminosity and surface brightness, as is the case for our models.

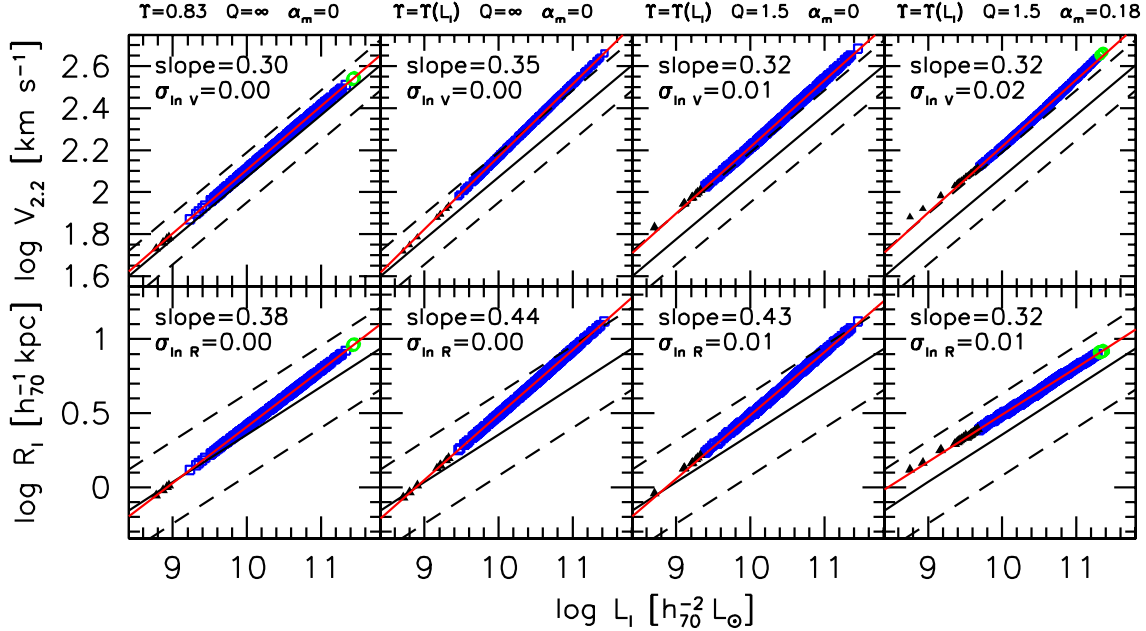


FIG. 6.— VL and RL relations using our fiducial mean c , λ_{gal} , and m_{gal} parameters and different values of Υ_l , Q and α_m . The black solid and dashed lines show the mean and 2σ scatter of the observations. The red line is a fit to the model galaxies, whose slope is given in the top left corner of each box. The color of the points corresponds to $\mu_{0,l}$ as in Fig. 1. The model on the far left is the MMW model with $\Upsilon_l = 0.83$, $Q = \infty$ (a pure stellar disk) and $\alpha_m = 0$. The model in the left middle only differs from this model in the Υ_l , which we assume follows Eq. 38. This steepens the slopes of the VL and RL relations making them incompatible with the data. The right middle model includes the star formation threshold, which results in a gas fraction that increases with decreasing luminosity, and hence a shallower VL slope, in agreement with the data. The effect on the RL slope is not as strong because as the luminosities are decreased, so are the stellar disk scale lengths. Notice that the star formation threshold has introduced a small curvature to both the VL and RL relations. In order to match the RL slope we set $\alpha_m = 0.18$ (far right panel). Although m_{gal} now varies significantly with luminosity, the only effect on the VL relation is to increase the curvature slightly. While this model matches the slope of the VL and RL relations it fails to reproduce the zero points.

4.1.2. Zero points

Having explored how some of our model parameters impact the slopes of the VL and RL relations, we now turn to the zero points, which we define as the values of V and R at the mean luminosity of our data; $\log L_l = 10.3$. For our reference model with $\alpha_m = 0.18$ which matches the slopes of the VL and RL relations, the model galaxies are both too large (by ~ 35 percent) and rotate too fast (by ~ 40 percent). This corresponds to a 2σ offset in terms of the observed scatter in the VL relation, and thus an even more significant offset in terms of the actual uncertainty in the VL zero point.

The inability of CDM based galaxy formation models to match the VL zero point is a generic problem that has been identified in numerical simulations (Elizondo et al. 1999; Navarro & Steinmetz 2000, Eke, Navarro & Steinmetz 2001; Sommer-Larsen et al. 2003), in semi-analytic models (e.g., Mo & Mao 2000; van den Bosch 2000, Firmani & Avila-Reese 2000; Cole et al. 2000; Benson et al. 2003) and in halo occupation models (Yang, Mo, & van den Bosch 2003). In particular no model has been able to simultaneously match the luminosity function and the zero point of the VL relation, using standard Λ CDM parameters. Cases that claim an agreement either assume that the observed rotation velocity, V_{obs} , is equal to V_{vir} (e.g., Somerville & Primack 1999), or to V_{max} (e.g. Croton et al. 2006). In both cases, the effect of the baryons on the rotation curve is completely ignored. As shown in Fig. 4, when adiabatic contraction of the dark matter halo and the disk's own contribution to V_{obs} are properly accounted for, one predicts that $V_{\text{obs}}/V_{\text{vir}} \simeq 1.7$ for a typical halo in a Λ CDM cosmology. Models that fail to take these effects into account can therefore not be used for a meaning-

ful comparison with the data (see also Navarro & Steinmetz 2000; van den Bosch 2000). For example, Croton et al. (2006) model V_{obs} as the maximum circular velocity of a NFW halo, V_{max} . As shown by the dot-dashed curve (labelled $V_{\text{max}}/V_{\text{vir}}$) in Fig. 4, this more or less corresponds to halo expansion with $\nu = -1.0$. We will return to the implications of this in §5.

In principle, there are a number of different ways in which one might envision solving the VL zero point problem:

1. Lower stellar mass-to-light ratios. This trivially increases the luminosity of the model galaxies at a fixed rotation velocity. For our reference model we need to lower Υ by $\simeq 0.5$ dex. However, the most that one can justify based on realistic IMFs is $\Delta_{\text{IMF}} \simeq -0.2$ dex (corresponding to a Kennicutt IMF), more than a factor of 2 smaller than what is required.
2. Lower halo concentrations. This results in a lower $V_{2,2}$ at a given L . Halo concentrations can be lowered by, for example, decreasing the cosmological parameters Ω_m and/or σ_8 . A reduction of the power spectrum on small scales also results in lower halo concentrations (Zentner & Bullock 2002). However, for our reference model to match the VL zero point we need $\eta_c \simeq 0.3$ which is difficult to reconcile with current constraints on cosmological parameters and the matter power spectrum.
3. Modify adiabatic contraction. As discussed in §3.2 a more realistic treatment of adiabatic contraction than the standard BFFP formalism is unlikely to have any significant impact on $V_{2,2}$. However, if we simply turn off adiabatic contraction (i.e. $\nu = 0$), $V_{2,2}$ will be lowered by $\simeq 20\%$. An even stronger reduction can be ac-

TABLE 2
MODEL PARAMETERS

Model	Δ_{IMF}	ν	η_c	Q	$\bar{\lambda}_{\text{gal}}$	$m_{\text{gal},0}$	α_m	β_{crit}	f_x
I	-0.40	0.8	0.80	1.5	0.042	0.06	0.25	0.66	0.25
II	-0.20	0.8	0.50	1.5	0.042	0.10	0.25	0.75	0.25
III	-0.20	0.0	0.80	1.5	0.042	0.09	0.25	0.80	0.25
IV	-0.20	-1.0	1.00	1.5	0.023	0.03	0.30	0.85	0.25

complished by considering expansion, modelled by setting $\nu < 0$ in Eq. (34).

Based on these possibilities we construct three models that match the *VL* and *RL* zero points and slopes. The parameters of these models are listed in Table 2. In each of these models we tune the parameter $m_{\text{gal},0}$ and α_m to fit the *RL* zero point and slope. Note that these models should only be considered specific examples of a more extended parameter space, which we describe in more detail in §5. These models mainly serve to highlight the various possible solutions to the *VL* zero point problem discussed above.

In model I we consider elements from all three modifications discussed above. We reduce the halo concentrations by 20% (i.e. we set $\eta_c = 0.8$), which corresponds to changing (Ω_m, σ_8) from $(0.3, 0.9)$ to $(0.25, 0.8)$, as advocated by van den Bosch, Mo & Yang (2003) and which is in agreement with the third year WMAP results (Spergel et al. 2006). In addition, we use the adiabatic invariant of Gnedin et al. (2004) which corresponds to $\nu = 0.8$. Finally, we adjust the stellar mass-to-light ratios until we match the zero-points, which requires $\Delta_{IMF} = -0.4$. As discussed above, such a large reduction in Υ_I implies an unrealistically top-heavy IMF. This model should therefore be considered as an illustration only. Because of the lower c and the reduced halo contraction, the resulting disk galaxies are larger than in our reference model. We counter-balance this by slightly increasing $m_{\text{gal},0}$ from our fiducial value of 0.05 to 0.06. Alternatively, we could have matched the increase in disk scale lengths by decreasing $\bar{\lambda}_{\text{gal}}$: such models are discussed in §5.

In model II we restrict Δ_{IMF} to -0.2 , which is the most we can accommodate with realistic IMFs, and we match the *VL* zero point by lowering c by 50%. As shown by Zentner & Bullock (2002), such a large reduction in halo concentrations can be reconciled with a power spectrum with a running spectral index that is still consistent with the WMAP data (Spergel et al. 2003).

Finally, in model III we simply turn off adiabatic contraction ($\nu = 0$). This model is able to match the *VL* and *RL* zero points with the standard $c(M_{\text{vir}})$ for a Λ CDM cosmology with $\Omega_m = 0.25$ and $\sigma_8 = 0.8$ (i.e., $\eta_c = 0.8$) and with a realistic IMF ($\Delta_{IMF} = -0.2$).

4.2. Models with Scatter

Having identified models that can simultaneously match the slopes and zero points of the *VL* and *RL* relations, we now focus on the scatter in both relations. The observed scatter in the *VL* and *RL* relations at fixed L_I are $\sigma_{\ln V} = 0.13$ and $\sigma_{\ln R} = 0.32$ respectively. The observational uncertainties are estimated to be $\sigma_{\ln V} \simeq 0.08$, $\sigma_{\ln L} \simeq 0.10$, and $\sigma_{\ln R} \simeq 0.14$ (see §2.1). Subtracting these in quadrature (with an error weighted scheme) from the observed scatter leaves an intrinsic scatter of $\sigma_{\ln V} = 0.12$ and $\sigma_{\ln R} = 0.28$. Note that our error weighted subtraction results in a slightly larger intrinsic scatter than obtained from a straight quadratic subtraction.

TABLE 3
SOURCES OF INTRINSIC SCATTER

	$\sigma_{\ln \Upsilon_I}$	$\sigma_{\ln c}$	$\sigma_{\ln \lambda}$	$\sigma_{\ln m_d}$
Maximum	0.32	0.40	0.25	0.55
Predicted	0.23	0.32	0.50	-
Adopted	0.23	0.23	0.25	0.00

NOTE. — The first row gives the maximum scatter in Υ_I , c , λ_{gal} , and m_{gal} that is consistent with the *VL* and *RL* scatter. The second row gives the predicted scatter, for c and λ_{gal} from cosmological simulations, for Υ_I from observations. The third row gives the scatter adopted in models I-III in order to match the *VL* and *RL* scatter simultaneously while including bulge formation.

The scatter in our models originates from four sources: Υ_I , c , λ_{gal} , and m_{gal} . Table 3 lists the expected amount of scatter in each of these four variables, and Fig. 7 shows the effect of these sources of scatter on the *VL* and *RL* relations. Lower c , higher λ_{gal} , and lower m_{gal} all result in larger scale lengths, and lower stellar masses and luminosities. Higher Υ_I result in lower luminosities, and higher effective (i.e. at a fixed luminosity) scale lengths. The fact that scatter in c and λ_{gal} also effects the luminosity is entirely due to the star formation threshold and results in a significantly reduced *VL* scatter due to λ_{gal} . As already discussed in §4.1.1, scatter in m_{gal} moves galaxies approximately parallel to the *VL* relation, but only for intermediate values of the galaxy mass fraction: for large m_{gal} scatter results in $V \propto L^{0.5}$, while for sufficiently low values of m_{gal} the corresponding slope approaches zero.

Fig. 7 also yields useful insight on the effect of the various parameters on the zero points of the *VL* and *RL* relations. The most effective way to change the *VL* zero point is to change the average halo concentration, c , or the average stellar mass-to-light ratio, Υ_I . The zero point of the *RL* relation, on the other hand, is most easily changed by a modification of the mean spin parameter, λ_{gal} , or the average galaxy mass fraction, m_{gal} .

4.2.1. Constraining the amount of scatter

To determine the maximum amount of scatter allowed for each parameter we run models with log-normal scatter in one of the four parameters only. We increase the scatter until we reach the intrinsic scatter of either the *VL* or *RL* relation. The resulting limits on the amounts of scatter in c , λ_{gal} , m_{gal} , Υ_I , are very similar for each of the three models discussed above. In Table 3 we list the representative values thus obtained. As expected from Fig. 7, the limits for Υ_I and c come from the *VL* relation, while those for λ_{gal} and m_{gal} owe to the *RL* relation. Note that the *expected* amounts of scatter (also listed in Table 3) in Υ_I and c are smaller, and therefore consistent with, their respective maximum amounts. In the case of the spin parameter, however, the expected amount of scatter is a factor two larger than the maximum amount allowed by the intrinsic scatter in the *RL* relation. This can have a number of important implications, of which we consider the following three:

1. Due to surface brightness selection effects our data is missing the lowest and/or highest surface brightness galaxies. Although this is certainly possible to some extent, gauging from the incompleteness corrections of de Jong & Lacey (2000) we conclude that these effects are likely to be small (Courteau et al. 2006).

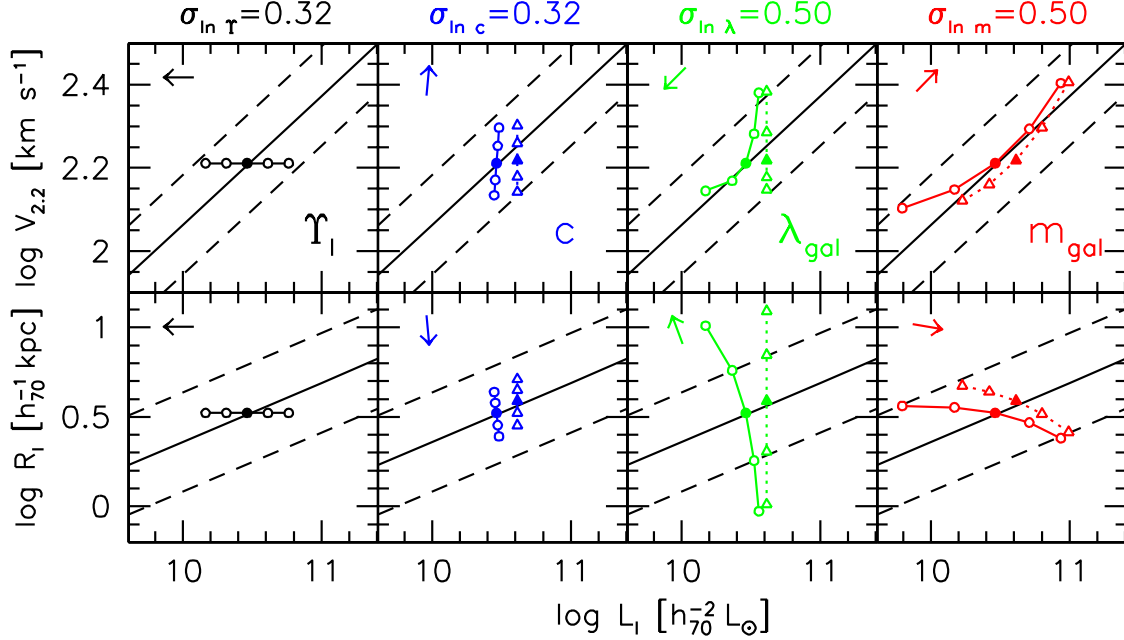


FIG. 7.— Contribution of scatter in Υ_I , c , λ_{gal} , and m_{gal} to the I-band VL and RL scaling relations for our reference model with $M_{\text{vir}} = 3 \times 10^{11} h^{-1} M_{\odot}$ and $\Delta_{\text{IMF}} = -0.5$ (to match the zero points). Models with/without the star formation threshold are given by circles/triangles. The solid symbol shows the mean parameter model, the open symbols show the models with ± 1 & 2σ scatter in the parameter. The arrow in the top left of each panel shows the direction in which the parameter increases. The observed mean and 2σ scatter are given by solid and dashed lines, respectively. See text for further details.

2. Disk galaxies acquire a narrower distribution of specific angular momentum than their host halos (i.e., the scatter in $\ln \lambda_{\text{gal}}$ is smaller than that in $\ln \lambda$). This can occur, for example, through the redistribution of angular momentum associated with bulge formation. We discuss such a possibility in the next section.
3. Disk galaxies form in a sub-set of halos with a smaller $\sigma_{\ln \lambda}$. Interestingly, this is expected if disk galaxies form mainly in those halos that have not experienced recent major mergers (D’Onghia & Burkert 2004). In addition to a smaller scatter in both λ and c , this subset of halos also has a significantly smaller mean spin parameter, and possibly a higher mean c (Wechsler et al. 2002). We discuss such a model in §5.

Having determined the maximum amounts of scatter allowed by the data, we now proceed to set their actual values. Since scatter in m_d does not contribute much scatter to the VL relation, and the scatter in the RL relation is already over-budgeted because of the spin parameter, we set $\sigma_{\ln m} = 0$ in what follows. In addition, we set the scatter in the stellar mass-to-light ratios to the expected amount, i.e., $\sigma_{\ln \Upsilon} = 0.23$. If we also set $\sigma_{\ln c}$ to its predicted value of 0.32, then the scatter in the VL relation is already larger than observed, even without any scatter in λ_{gal} . We therefore adopt $\sigma_{\ln c} = 0.23$, which is the value predicted for halos that have not experienced any recent major mergers (Wechsler et al. 2002). Finally, we tune the scatter in λ_{gal} until we match the observed scatter in the RL relation, which yields $\sigma_{\ln \lambda} = 0.25$ (when including bulge formation, see below). Throughout this paper we treat c , Υ_I , m_{gal} and λ_{gal} as independent variables. In reality, the scatter in some of these parameters may be correlated. In Appendix B we discuss possible correlations, and how they impact on our results.

4.2.2. Bulge Formation

Thus far we have only considered models without bulge formation (i.e., with $\beta_{\text{crit}} = 1$ in Eq. (31)). We now introduce bulge formation to the three models described above. We set $f_x = 0.25$, and tune β_{crit} so that the sample of model galaxies has the same mean bulge-to-disk ratio as the data ($\simeq 0.15$). None of our results are sensitive to the exact value of f_x chosen.

Since m_{gal} increases and c decreases with halo mass, more massive halos typically host galaxies with a larger β_{max} . Also, for a given halo mass, the disk’s contribution to the circular velocity increases with decreasing spin parameter λ_{gal} . Consequently, it is predominantly the luminous, high surface brightness galaxies residing in massive halos that will form a bulge in our models.

Bulge formation only has a small effect on the VL relation, but does cause a modest change of the RL relation. For our fiducial value of f_x , and in fact for all $f_x \lesssim 1$, bulge formation causes an increase of the specific angular momentum of the disk, and thus of its scale length. Since bulge formation preferentially affects the galaxies in the lower right part of the RL plane (i.e. the highest surface brightness galaxies), this will actually reduce the scatter in the RL relation at the bright end (see also Shen et al. 2003). At the faint end no bulges form, so that this also causes a small increase in the slope of the RL relation, which we counter by increasing α_m . For realistic bulge-to-disk ratios the overall scatter in the RL relation is reduced at most by $\simeq 15\%$. Although this also changes the maximum amounts of scatter allowed by the data by a similar fraction, the maximum scatter in λ_{gal} allowed by the RL scatter is never larger than 0.3, which is still much smaller than the predicted amount. Thus bulge formation is not able to reconcile the expected scatter in λ with that of the observed scatter in the RL relation.

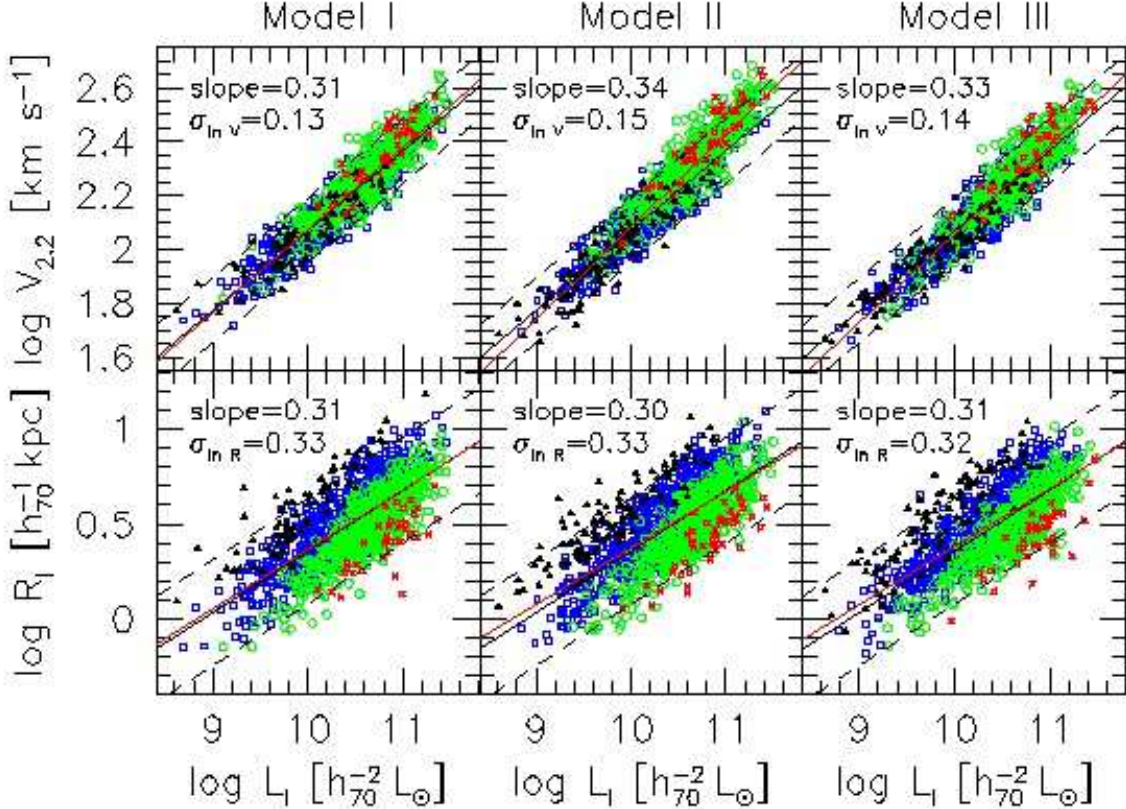


FIG. 8.— I-band VL and RL scaling relations for our three models with bulge formation and scatter in c , λ_{gal} , Υ_I and observational errors. The parameters of these models are given in Table 2. The black solid and dashed lines show the mean and 2σ scatter of the data, respectively. The solid red lines give the mean relation of the model galaxies from unweighted least-squares fits of V on L and R on L . The colors and point types correspond to surface brightness as in Fig. 1. Each model sample consists of $\simeq 1300$ galaxies, sampled to reproduce the observed distribution of luminosities.

The VL and RL relations for models I-III with bulge formation, scatter in c , λ_{gal} , Υ_I , and observational errors are shown in Fig. 8. Overall, all three models provide a reasonable match to the slopes, zero points and scatter of the observed relations. A detailed comparison with Fig. 1, however, reveals that all three models, but especially Model II, have a slight problem at the bright end where they predict rotation velocities that are somewhat too high. This is related to the fact that the contribution of the baryons to $V_{2.2}$ increases with luminosity (see §4.3.2). Consequently, the VL relation deviates from a pure power-law. As we will see in §4.3 below, this causes a weak, but significant correlation between surface brightness and the VL residual.

4.3. Residual correlations

Models I, II and III all fit the slopes, zero points and the amounts of scatter of the VL and RL relations. An important question is whether we can discriminate between these three models, or whether there are genuine degeneracies in the model parameter space. As shown in Fig 2 there is additional information in the residual correlations. In particular, the residuals in the VL and RL relations are virtually uncorrelated, so that the VL residuals are not significantly correlated with surface brightness (CR99). We now investigate how models I, II and III fare in matching these aspects of the data.

The upper panels of Fig. 9 show the residuals of the RL relations of models I-III plotted against central surface brightness. All three models are virtually indistinguishable, and

accurately reproduce the data (upper-left panel of Fig. 2). This, however, owes simply to the luminosity sampling of the data, which we reproduce using a Monte-Carlo technique (see §2.2). The lower panels of Fig. 9, however, plot the VL residuals against central surface brightness. This time, the three models differ slightly from each other, and significantly from the data. All models predict a small but non-negligible correlation between surface brightness and the VL residual, contrary to the data (lower-left panel of Fig. 2). This owes mainly to the non power-law character of the model VL relations, as discussed above.

The upper panels of Fig. 10 show the VL residuals as function of the RL residuals. Except for Model II, which predicts a correlation slope $\gamma \equiv d[\Delta \log V(L)]/d[\Delta \log R(L)]$ which is somewhat too steep, these residual correlations are in good agreement with the data (lower-right panel of Fig. 2).

As discussed in §1, the absence of a pronounced correlation between the VL and RL residuals is contrary to naive expectations. In order to understand which aspects of the model cause this success, we start by considering the model *baryonic* VM and RM relations (i.e. velocity at 2.2 baryonic scale lengths vs. baryonic mass and baryonic scale length vs. baryonic mass). The lower panels of Fig. 10 show that the residuals of these baryonic scaling relations are strongly correlated, for each of the three models. This owes to the fact that a smaller λ_{gal} implies both a reduction of the disk scale length and an increase in $V_{2.2}$. Thus, the naive expectation that the residuals should be correlated at least holds for the baryonic scaling relations. We find this to be a very generic predic-

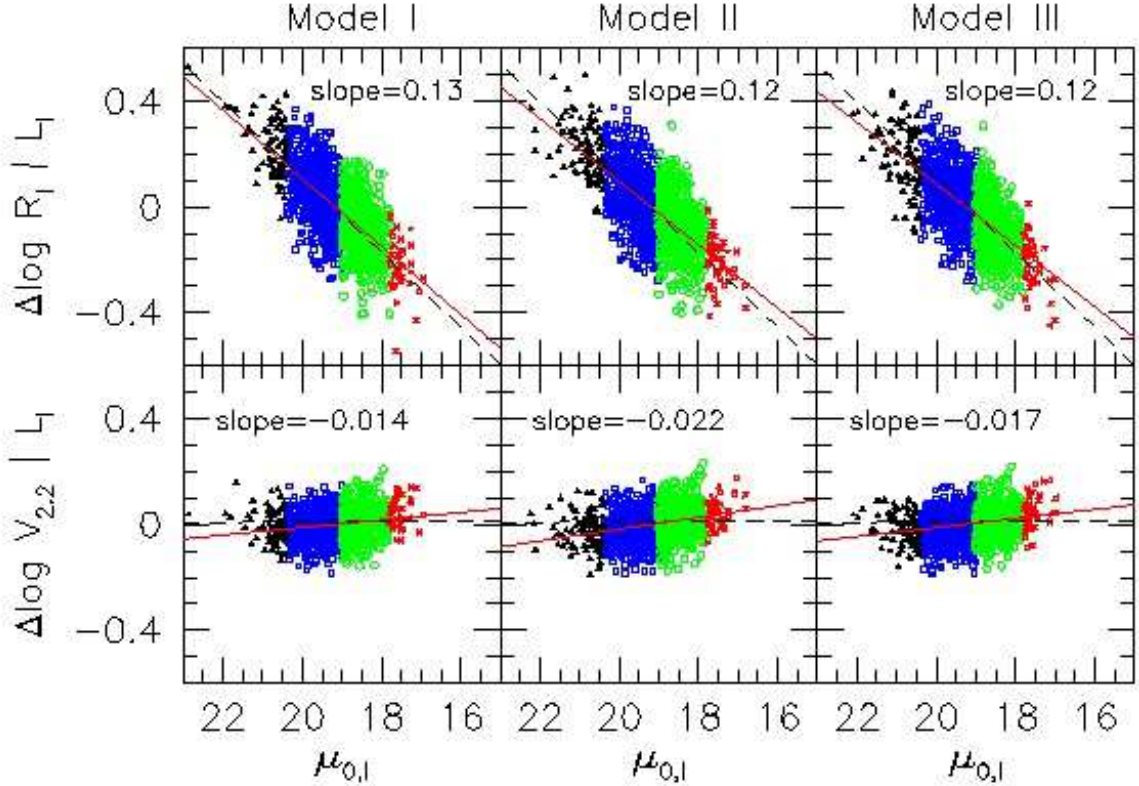


FIG. 9.—Residuals of the model *I*-band *VL* and *RL* relations versus surface brightness, for models in Fig. 8. The observed relations are given by the dashed line. All three models reproduce the surface brightness dependence of the *RL* relation, but none of the models are able to reproduce the observed surface brightness independence of the *VL* relation.

tion of our models, even though the exact value of the slope of the baryonic residual correlation may vary somewhat from model to model. Although measuring baryonic masses and baryonic sizes depends on stellar mass-to-light ratios, which are difficult to constrain on a galaxy by galaxy basis, these can be determined in a statistical sense for a suitably chosen sample. Thus, in principle the baryonic scaling relations are observable, and our predictions regarding their residual correlations provide a useful test for our models. We caution, however, that it is crucial that the rotation velocity is measured at 2.2 disk scale lengths. For example, when V is measured at 5 disk scale lengths, our models predict a significantly shallower residual correlation.

The middle panels of Fig. 10 show the residual correlations from the model *stellar* mass *VM* and *RM* relations (i.e. velocity at 2.2 stellar scale lengths vs. stellar mass and stellar scale length vs. stellar mass). Note that the strength of these correlations is significantly reduced with respect to the baryonic case (lower panels). This is caused by the star formation threshold, which correlates the stellar mass at a given baryonic mass to the spin parameter: a lower λ_{gal} not only results in a smaller scale length and a larger $V_{2,2}$, it also results in a relatively larger stellar mass, therewith reducing the residual correlation. This, together with the constraint of matching the slope of the *VL* relation, is another argument in favor of including a star formation threshold (or something equivalent) in our models. In fact, FA00 argued that a star formation threshold density is the main explanation for the weak residual correlation observed. Although we agree that it substantially reduces the residual correlations, it does not automatically re-

sult in uncorrelated residuals, as is evident from the middle panels of Fig. 10. The weaker correlation between the *VL* and *RL* residuals in the upper panels compared with the middle panels in Fig. 10 is achieved through scatter in Υ_I and, to a lesser extent, to our modelling of the observational errors in V , L and R .

4.3.1. Impact of Scatter

To gauge how the various sources of scatter impact the residual correlations, Fig. 11 shows $\Delta \log V$ against $\Delta \log R$ for models that have only scatter in one of the four parameters: Υ_I , c , λ_{gal} , or m_{gal} . The spin parameter, λ_{gal} , and the galaxy mass fraction, m_{gal} , only cause significant scatter in the *RL* relation. Consequently, they result in residual correlations with $|\gamma| \lesssim 0.1$, in agreement with the data, which has $\gamma = -0.08 \pm 0.03$ (see §2.2). Scatter in c and Υ_I , however, predict strongly correlated residuals with $\gamma \simeq -0.6$ and $\gamma \simeq 1$, respectively.

Thus, achieving *VL* and *RL* relations with uncorrelated residuals requires a subtle balance between the amounts of scatter in the halo concentrations, c , and the stellar mass-to-light ratios, Υ_I . To emphasize this point, Fig. 12 shows the residual correlations for models with different amounts of scatter in c and Υ_I . The scatter in λ_{gal} and the scatter due to observational errors are kept constant. A model with only scatter in λ_{gal} and observational errors has $\gamma = -0.06$. Including the maximum amount of scatter in c (middle panel) results in a strong negative correlation, $\gamma = -0.19$. In contrast, including the maximum scatter in Υ_I , with no scatter in c , results in a weak, positive correlation with $\gamma \simeq 0.06$ (right panel). In practice scatter in both c and Υ_I are expected to contribute to

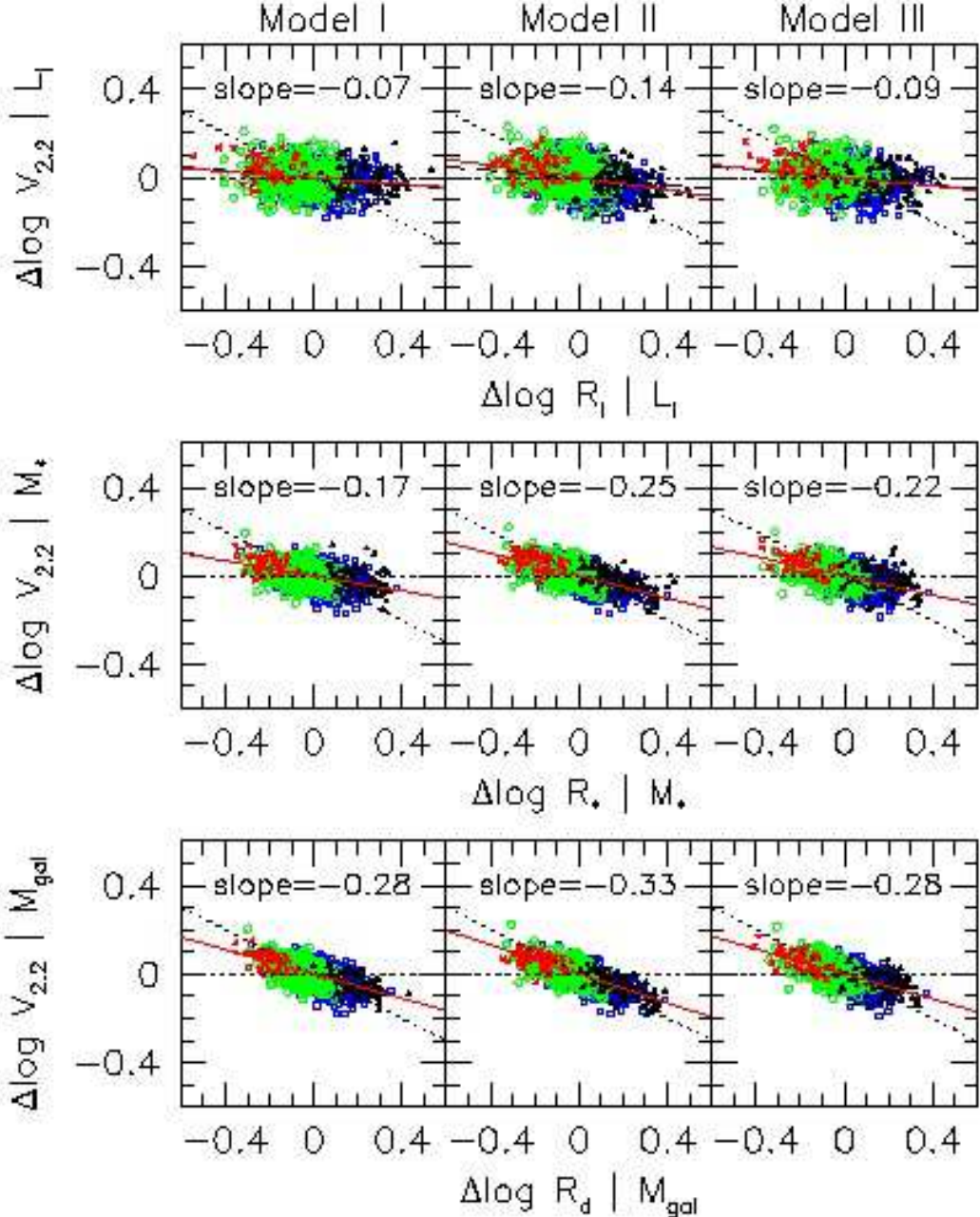


FIG. 10.— Residual correlations for our three models. The upper panels show the residuals of the I -band VL and RL relations, the middle panels show the residuals of the stellar mass VM and RM relations, while the lower panels show the residuals of the baryonic mass VM and RM relations. The solid red lines show the fits of ΔV on ΔR . The dotted lines show slopes of 0 and -0.5. For the upper panels we show the observed correlation as long-dashed lines. Notice that the correlation between the residuals decreases in magnitude going from the baryonic mass to stellar mass to I -band luminosity.

the VL scatter, so there is not much freedom to tune the residual correlations. In order to reproduce the total VL scatter we adopted $\sigma_{\ln c} = \sigma_{\ln \gamma} = 0.23$. As shown in Figs. 9 & 10, this amount of scatter results in a weak residual correlation and a small but significant surface brightness dependence to the VL scatter. Removing these dependences entirely would require a larger scatter in γ_I and a lower scatter in c . The former is feasible, but the latter would require an even more biased subset of halos than just those without recent major mergers.

4.3.2. Dark and baryonic mass fractions

The upper panels of Fig. 13 show the ratio $V_{\text{gal}}/V_{2.2}$ as function of surface brightness for all three models. Here V_{gal} and $V_{2.2}$ are the circular velocities of the baryons (disk plus bulge) and the total mass distribution (baryons plus dark matter) respectively, both measured at 2.2 disk scale lengths. The solid, horizontal line indicates β_{crit} : all galaxies above this line contain a bulge component (whose contribution to $V_{2.2}$ is given by the magenta triangles). Since we tuned β_{crit} to match the mean bulge-to-disk ratio of the data, its value is different for different models.

In all 3 models, $V_{\text{gal}}/V_{2.2}$ is strongly correlated with surface brightness, and to a lesser extent luminosity (middle pan-

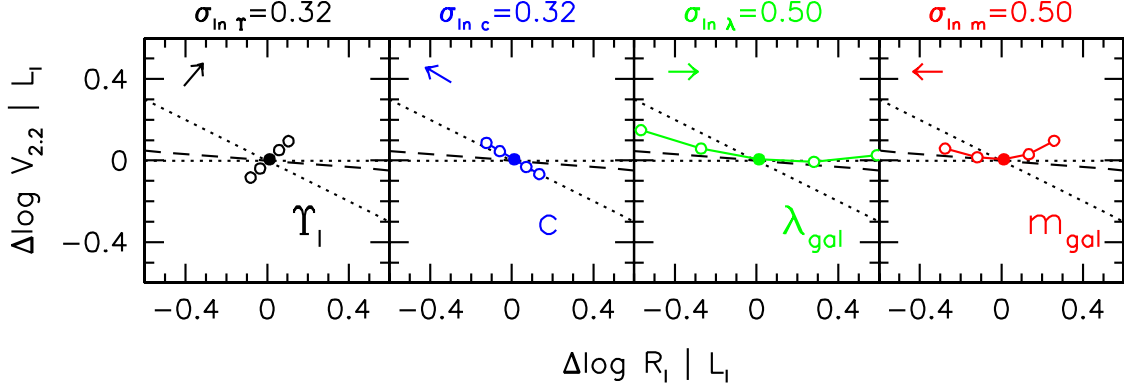


FIG. 11.— Contribution of scatter in Υ_I , c , λ_{gal} , and m_{gal} to the residual correlation for our reference model with $M_{\text{vir}} = 3 \times 10^{11} h^{-1} M_{\odot}$ and $\Delta_{\text{IMF}} = -0.5$ (see also Fig. 7). The solid dot shows the mean parameter model, the open circles show the models with ± 1 & 2σ of the scatter given at the top of each panel. The arrow in the top left of each panel shows the direction of increasing parameter. The observed slope is shown by the dashed line; the dotted lines have slopes of 0 and -0.5. A slope of -0.5 is expected for a pure exponential disk (CR99).

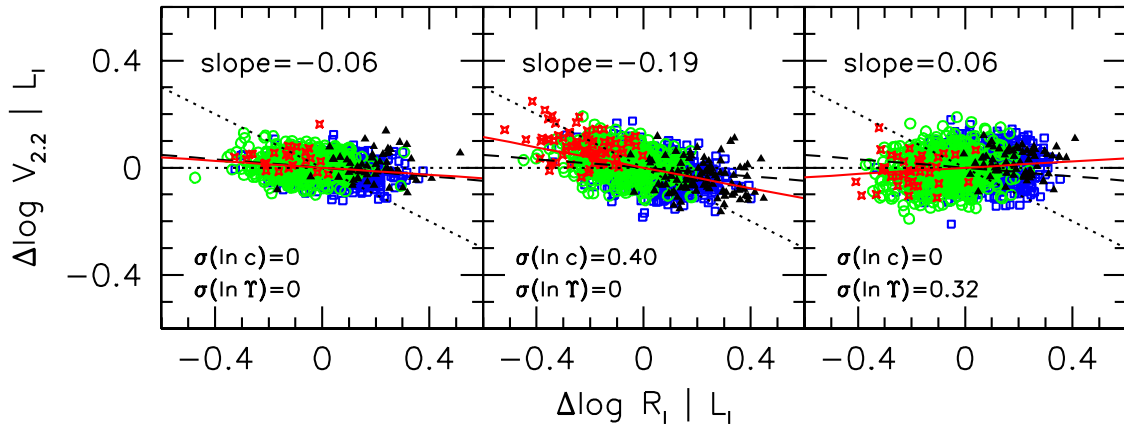


FIG. 12.— Residual correlations for Model I with different amounts of scatter in Υ_I and c . All panels are computed with $\sigma_{\ln \lambda} = 0.25$, and observational errors. The model on the left has zero scatter in c and Υ_I , and a weak negative residual correlation consistent with the data. The model in the middle has maximum scatter in c , this results in a significant negative residual correlation. The model on the right has maximum scatter in Υ_I , this results in a slight positive residual correlation. Thus larger scatter in Υ_I and lower scatter in c help to reduce the magnitude of the residual correlation.

els; see also FA00 and Zavala et al. 2003). In fact, most of the luminosity dependence simply owes to the fact that more luminous galaxies typically have a higher surface brightness, as is evident from the color-coding. Note that the mean $V_{\text{gal}}/V_{2.2}$ is significantly different for different models. In the case of Model I (top-heavy IMF), there are no galaxies with $V_{\text{gal}}/V_{2.2} > 0.85$ (indicated by the gray shaded region). This means that, in this model, the baryons never contribute more than ~ 70 percent of the total enclosed mass within $2.2R_d$. In models II and III the fraction of galaxies with $V_{\text{gal}}/V_{2.2} > 0.85$ are $\simeq 4\%$ and $\simeq 37\%$, respectively. Note that Models I and III, though, have a very similar residual correlation slope γ (upper panels of Fig. 10). This is in contradiction to CR99 who argued that γ is uniquely correlated with the mean $V_d/V_{2.2}$; in particular, from the weak residual correlation observed, they concluded that high surface brightness disk galaxies should have, *on average* $V_d/V_{2.2} \simeq 0.6$. In Appendix C we discuss the CR99 method in more detail, and show why the observed value of γ does not accurately constrain $V_d/V_{2.2}$.

Finally, the lower panels of Fig. 13 show the ratio $V_{2.2}/V_{\text{vir}}$ as a function of luminosity. Note that the circular velocity at 2.2 disk scale lengths can be as large as two times the virial

velocity. The median values of $V_{2.2}/V_{\text{vir}}$ are 1.68, 1.86 and 1.67 for Models I, II, and III, respectively. As we discuss in more detail in §5.1 below, these relatively high values have important implications.

5. LOW SPIN PARAMETER MODELS

As discussed the zero point of the RL relation is highly degenerate between changes in $\bar{\lambda}_{\text{gal}}$ and $m_{\text{gal},0}$. In §4 we chose to tune m_{gal} in order to match the RL relation, while keeping $\bar{\lambda}_{\text{gal}}$ fixed at the median value of the spin parameter of dark matter halos; $\bar{\lambda}_{\text{gal}} = \bar{\lambda} = 0.042$. However, there are several reasons why one might expect that the spin parameter of the galaxy is different from that of its dark matter halo. Firstly, numerical simulations suggest that haloes that are more likely to host disk galaxies, i.e., those that did not experience any recent major mergers, have a median spin parameter that is significantly lower than that of the full distribution of haloes (D’Onghia & Burkert 2004; Macciò et al. 2006). Secondly, mass is generally more centrally concentrated than specific angular momentum. Consequently, if disks form inside out, one expects that $j_{\text{gal}} < m_{\text{gal}}$, and thus $\lambda_{\text{gal}} < \lambda$. Thirdly, during galaxy formation angular momentum may be transferred from

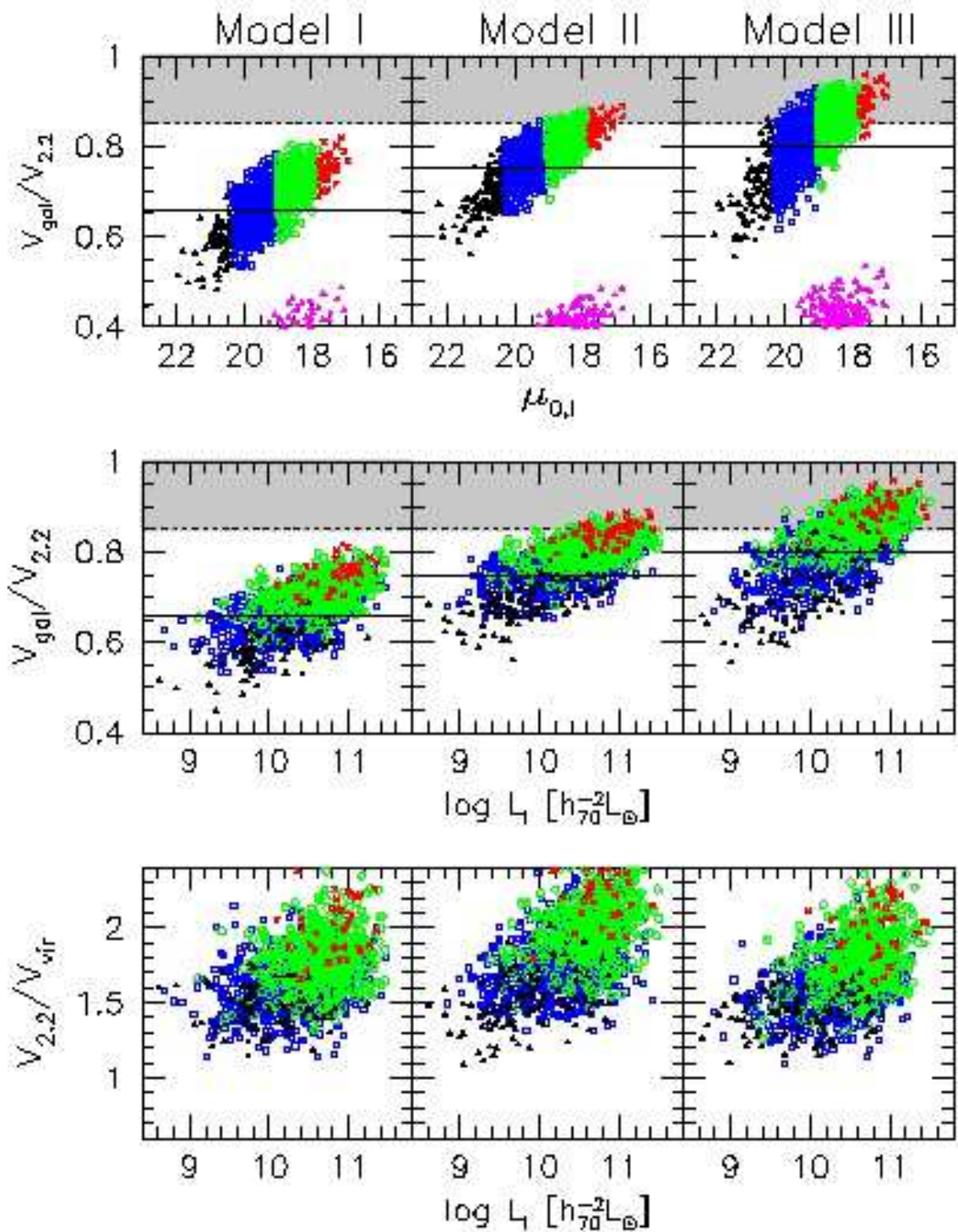


FIG. 13.— Contribution of the baryons (stellar disk, gaseous disk, and bulge) to circular velocity at 2.2 disk scale lengths, $V_{\text{gal}}/V_{2,2}$, and ratio of observed to virial circular velocity for Models I, II, & III. Point types and colors are the same as in Fig. 1. All models show a strong dependence of $V_{\text{gal}}/V_{2,2}$ with surface brightness (upper panels), and a weaker one with luminosity (middle panels). The dependence on luminosity is mostly because more luminous galaxies have higher surface brightness. The horizontal dotted line shows $V_{\text{gal}}/V_{2,2} = 0.85$, the shaded region above this line corresponds to galaxies that are baryon dominated within 2.2 disk scale lengths. Note however that due to our bulge formation recipe the contribution of the disk to \dot{V}_{gal} is always less than 0.85. The maximum contribution of the disk to V_{gal} is given by the horizontal black solid line. The contribution of the bulge is shown by the magenta triangles, and in all cases contributes less than $\simeq 25\%$ of the total mass within 2.2 disk scale lengths. The lower panels show $V_{2,2}/V_{\text{vir}}$ against luminosity. The median $V_{2,2}/V_{\text{vir}}$ for these model I, II, & III are 1.68, 1.86, & 1.67 respectively.

the baryons to the halo via dynamical friction, also resulting in $\lambda_{\text{gal}} < \lambda$. Finally, numerical simulations have shown that the *directions* of the angular momentum vectors of the (hot and cold) baryons and the dark matter can be strongly misaligned (van den Bosch 2002; Chen et al. 2003; Sharma & Steinmetz 2005; Bailin et al. 2005b), suggesting that λ and λ_{gal} are only poorly correlated.

To fully explore these possibilities, we relax the constraint that $\bar{\lambda}_{\text{gal}} = \bar{\lambda} = 0.042$ and investigate which combinations of λ_{gal} and m_{gal} match the zero points of the *VL* and *RL* relations. Our strategy is to run a grid of models in $m_{\text{gal}}\text{-}\lambda_{\text{gal}}$ space while keeping all other parameters fixed. In particular, we set $Q = 1.5$, $\Delta_{\text{IMF}} = -0.2$, and $\beta_{\text{crit}} = 1$. For a given combination of the concentration normalization, η_c , and the adiabatic contraction parameter, ν , we compute the zero point offsets from the observed *VL* and *RL* relations. We set the zero point to $\log L_I = 10.3$. Rather than compute a full model for each λ_{gal} and m_{gal} , we find the values of M_{vir} that result in $\log L_I = 10.3$. This requires an iterative procedure since the stellar mass fraction, and hence the luminosity, depend on λ_{gal} . In order to facilitate the interpretation of the zero point offsets we normalize them to the observed scatter in the *VL* and *RL* relations, respectively. The results of these grid searches are shown in Fig. 14. Each row corresponds to a model with a different η_c and ν , as indicated.

Panels in the first and second columns from the left show the constraints on λ_{gal} and m_{gal} from the *VL* zero points and the *RL* zero point, respectively. For the *RL* relation, there is a strong degeneracy in all models with $\lambda_{\text{gal}} \propto m_{\text{gal}}^{0.5}$; however, for a given m_{gal} the constraint on λ_{gal} is very strong. The third column from the left shows the quadratic sum of the *VL* and *RL* offsets, with contours as in the first two columns. The solid black dot shows the minimum of the *VL* + *RL* offset for each model within our grid, so it is not necessarily a global minimum. The fourth column from the left shows the ratio of the circular velocity of the baryons to the total circular velocity at 2.2 disk scale lengths, $V_{\text{gal}}/V_{2.2}$. Lines of constant $V_{\text{gal}}/V_{2.2}$ are approximately $\lambda_{\text{gal}} \propto m_{\text{gal}}$. In these models $V_{\text{gal}}/V_{2.2}$ is equivalent to central surface brightness, so that galaxies with low surface brightness disks have low $V_{\text{gal}}/V_{2.2}$, and vice versa for high surface brightness disks. The fifth column from the left shows the ratio of $V_{2.2}$ to V_{vir} . The dependence of this ratio on m_{gal} and λ_{gal} is more complicated than $V_{\text{gal}}/V_{2.2}$ but follows the same trend that models with higher m_{gal} and lower λ_{gal} have higher $V_{2.2}/V_{\text{vir}}$. Thus for model galaxies that match the *RL* zero point, lower λ_{gal} solutions have lower $V_{\text{gal}}/V_{2.2}$ and $V_{2.2}/V_{\text{vir}}$. We discuss the significance of this result below.

The first row uses the standard halo concentrations ($\eta_c = 1.0$) for a Λ CDM concordance cosmology ($\Omega_m = 0.3$, $\Omega_\Lambda = 0.7$, $\sigma_8 = 0.9$) and standard adiabatic contraction ($\nu = 1.0$). Note that the standard model advocated in MMW, which has $m_{\text{gal}} = \lambda_{\text{gal}} = 0.05$, predicts a *VL* zero point that is offset from the data by $\sim 2\sigma$. Matching the *VL* zero point for these values of η_c and ν requires $m_{\text{gal}} \simeq \lambda_{\text{gal}} \simeq 0.1$. However, this clearly results in disks that are too large. This demonstrates that this ‘standard’ model is unable to simultaneously match the *VL* and *RL* zero points for realistic Υ_I .

The second row shows a model with $\eta_c = 0.5$, i.e. with halo concentrations that are 50% lower than for the Λ CDM concordance cosmology. Although one can now match the *VL* zero point with smaller, more realistic λ_{gal} , a simultaneous match to the *VL* and *RL* zero points still requires relatively high m_{gal} . This is essentially Model II. As shown in the third

row of Fig. 14, very similar results are obtained for models with standard halo concentrations ($\eta_c = 1$) but without adiabatic contraction ($\nu = 0$). Model III is basically an example of such a model, which indeed yields results that are very similar to those of Model II.

In the fourth row we consider an even more unorthodox model; in addition to ‘turning off’ adiabatic contraction ($\nu = 0$), we also set the halo concentrations to be 50% lower than expected in the Λ CDM concordance cosmology ($\eta_c = 0.5$). For these parameters, the *VL* zero point can be matched for a very wide range of λ_{gal} and m_{gal} . In fact, there are two branches in $m_{\text{gal}}\text{-}\lambda_{\text{gal}}$ space that match the *VL* zero point, corresponding to high and low surface brightness disks. This branching is also visible from the curvature of the λ_{gal} and m_{gal} lines in the upper right panels of Fig. 7. In order to also match the *RL* relation the model needs to fall on the high surface brightness branch, and needs to have values for both λ_{gal} and m_{gal} that are much lower than for the previous models. Similar constraints are obtained for a model with halo expansion ($\nu = -1$) but with standard halo concentrations ($\eta_c = 1$), shown in the fifth row.

The lower two rows of panels thus indicate that there is a part of parameter space that can match the *VL* and *RL* zero points equally well as models I-III, but with a much lower average spin parameter and much lower galaxy mass fractions. Before we address the physical relevance of these unconventional models, we investigate to what extent they can match the *VL* and *RL* slopes and their residual correlations. Fig. 15 shows scaling relations and residual correlations for one particular model (hereafter Model IV) with halo expansion and standard concentrations, which matches both the *VL* and *RL* zero points. The parameters of this model are listed in Table 2, for the scatter in the model parameters we adopt $\sigma_{\ln c} = \sigma_{\ln \Upsilon} = 0.23$ (as for models I-III) and $\sigma_{\ln \lambda} = 0.28$. The median galaxy spin parameter is $\bar{\lambda}_{\text{gal}} = 0.023$, which is similar to the median spin parameter of dark matter halos that have not had a recent major merger (D’Onghia & Burkert 2004), while $m_{\text{gal},0} = 0.03$. Both of these values are much lower than for models I-III. Note that this model fits the slopes, zero points, scatter and correlation between residuals of the *VL* and *RL* relations. It also predicts a significant correlation between the residuals of the corresponding baryonic scaling relations, in agreement with Models I-III. The average $V_{\text{gal}}/V_{2.2}$ of this model is even larger than for Model III ($\simeq 62\%$ percent of all galaxies have $V_{\text{gal}}/V_{2.2} > 0.85$), indicating that a larger fraction of galaxies is baryon dominated within 2.2 disk scale lengths.

Finally, the lower-left panel of Fig. 15 plots $V_{2.2}/V_{\text{vir}}$ as function of the galaxy *I*-band luminosity. This model predicts an average $V_{2.2}/V_{\text{vir}}$ of ~ 1.2 , significantly lower than for models I-III. Thus, $V_{2.2}$ in Model IV is comparable to V_{max} , the maximum circular velocity of a NFW halo without adiabatic contraction (see Fig. 4). This is also evident from the panels in the fifth column of Fig. 14, which shows contours of constant $V_{2.2}/V_{\text{vir}}$: note that the models in the upper three rows that simultaneously match the *VL* and *RL* zero points, indicated by a solid dot, all predict relatively high values of $V_{2.2}/V_{\text{vir}}$ with a mean of $\simeq 1.8 \pm 0.1$. However, the models in the lower two rows, which can simultaneously fit the *VL* and *RL* zero points with low λ_{gal} and m_{gal} , predict much lower values of $V_{2.2}/V_{\text{vir}}$ with a mean of $\simeq 1.2$.

5.1. A revised model for disk formation

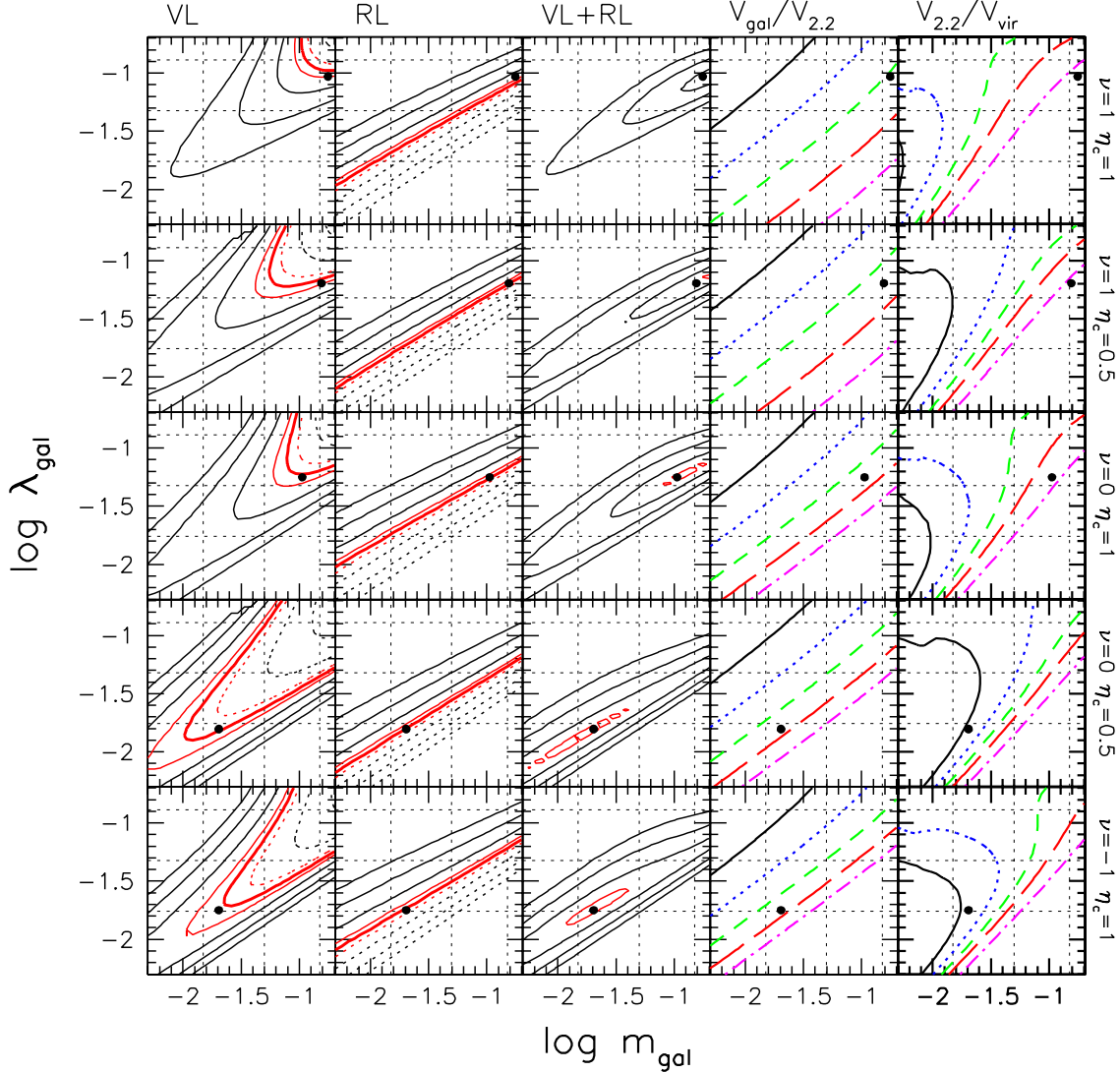


FIG. 14.— Parameter space of models for $0.005 \leq m_{\text{gal}}, \lambda_{\text{gal}} \leq 0.2$. All models assume $\Delta_{\text{IMF}} = -0.2$ and have no bulge formation. The horizontal lines show $\lambda_{\text{gal}} = 0.018, 0.048, \& 0.129$ (the mean and 2σ scatter in λ for cosmological DM halos). The vertical dotted lines show $m_{\text{gal}} = 0.015, 0.05, \& 0.15$ corresponding to $\simeq 10\%, 33\% \& 100\%$ galaxy formation efficiency. Each row corresponds to a different combination of adiabatic contraction, ν , and concentration normalization, η_c . The first and second columns show the offsets from the VL and RL relations at $\log L_t = 10.3$, with respect to the observed scatter in these relations. The black contours correspond to 1, 2, & 3 times the observed scatter. The red contours show 0.3 times the observed scatter, which is approximately the observed uncertainty in the zero points. The thick red line corresponds to no offset. Positive offsets are contoured with solid lines, while negative offsets are contoured with dotted lines. The third column shows the quadratic sum of the VL and RL offsets. The solid black dot shows the minimum of the VL+RL offset within our grid for each model. The fourth column gives the ratio of the circular velocity of the disk to the total circular velocity at 2.2 disk scale lengths, $V_d/V_{2.2}$: 0.95 (magenta dot-short dashed); 0.87 (red long dashed); 0.71 (green short dashed); 0.5 (blue dotted); 0.3 (black solid). The fifth column gives the ratio of the circular velocity at 2.2 disk scale lengths to the circular velocity at the virial radius, $V_{2.2}/V_{\text{vir}}$: 2.0 (magenta dot-short dashed); 1.6 (red long dashed); 1.4 (green short dashed); 1.2 (blue dotted); 1.0 (black solid). The top row uses standard adiabatic contraction, $\nu = 1$, and concentration parameters, $\eta_c = 1$: The second row also uses standard adiabatic contraction, but concentration parameters a factor 2 lower than the Bullock et al. (2001a) model, $\eta_c = 0.5$. The third row shows a model without adiabatic contraction, $\nu = 0$, but standard concentrations, $\eta_c = 1$. In order to match the zero points with low λ_{gal} , we need to either reduce the concentration, $\eta_c = 0.5$ (fourth row), or have expansion of the halo, $\nu = -1$ (fifth row).

We have shown that one can construct models that match the slopes, zero points and residual correlations of the VL and RL relations, and which predict relatively low values for $V_{2.2}/V_{\text{vir}}$. This has an important implication: all semi-analytic models that are able to match the luminosity function (LF) require $V_{\text{vir}} \lesssim V_{2.2} \lesssim V_{\text{max}}$ in order to simultaneously match the VL zero point (e.g., Somerville & Primack 1999; Cole et al. 2000; Benson et al. 2003; Croton et al. 2006). A similar conclusion was obtained by Yang et al. (2003) and van den Bosch et al. (2003) using the conditional luminosity function formalism. This suggests that models I-III will be unable to

simultaneously fit the observed LF of galaxies. Model IV, however, which is based on halo expansion, predicts ratios of $V_{2.2}/V_{\text{vir}}$ that clearly allow for a simultaneous fit to the LF. In more general terms, as can be seen from the fifth row of panels in Fig. 14, low values of $V_{2.2}/V_{\text{vir}}$ require average values for λ_{gal} and m_{gal} that are much lower than the standard values normally adopted. In the standard model (i.e., $\nu = 1$, $\eta_c = 1$), however, such low values for λ_{gal} and m_{gal} result in a VL zero-point that is in violent disagreement with the data. The only models for which a low $V_{2.2}/V_{\text{vir}}$ simultaneously allows a fit to both the VL and RL zero points are those in

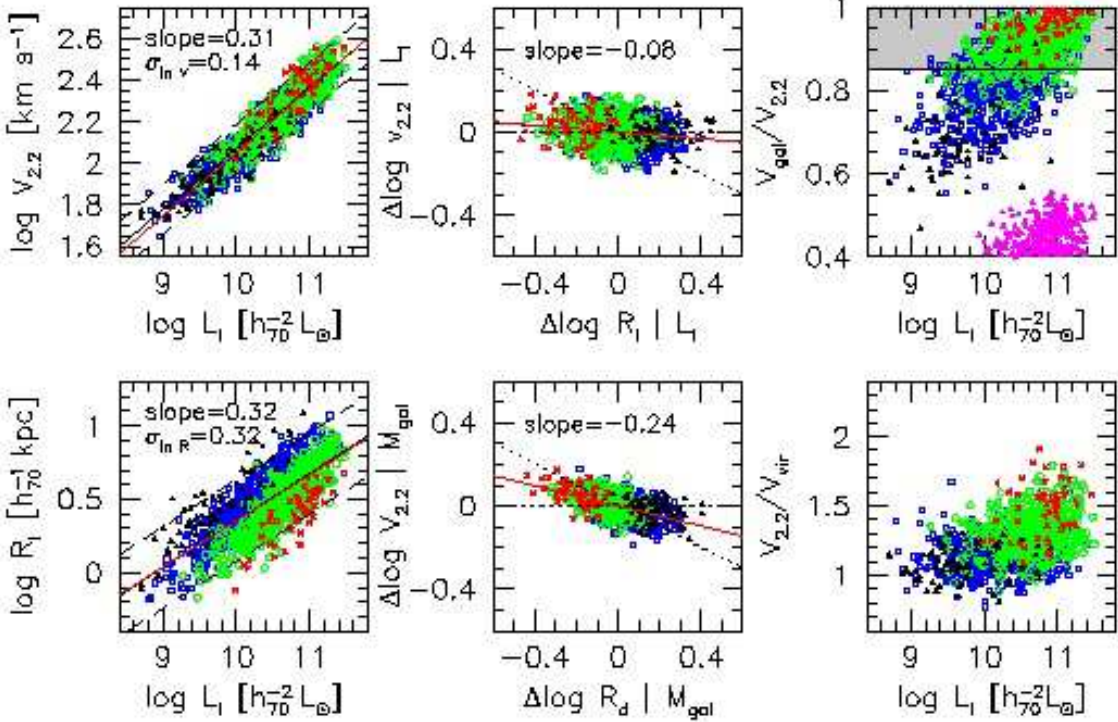


FIG. 15.— Scaling relations and residual correlations of model IV. This model reproduces the slopes, scatter and zero points of the VL and RL relations as well as the weak residual correlation. As with models I, II, & III, model IV predicts that the residuals of the baryonic mass VM and RM relations should be strongly anti-correlated. This model contains both baryon and dark matter dominated galaxies at 2.2 disk scale lengths, and has a median $V_{2.2}/V_{\text{vir}} = 1.22$ which is often required in order to simultaneously fit the luminosity function and the VL relation.

the lower two rows: either adiabatic contraction does not occur ($\nu = 0$) and halo concentrations are a factor two smaller than predicted for a Λ CDM concordance cosmology, or halos actually expand during disk formation (with $\nu \simeq -1$), in which case their original (before expansion) concentrations can be as predicted. Of course, one can also construct models with intermediate values of ν and η_c . For a cosmology with ($\Omega_m = 0.25, \sigma_8 = 0.75$) as advocated by the third year WMAP results (Spergel et al. 2006) $\eta_c = 0.75$ which requires $\nu \simeq -0.5$.

This obviously raises the question whether halo expansion during disk formation is a realistic option from a physical point of view. It is certainly inconsistent with the standard picture, in which disks form out of cooling flows that preserve their specific angular momentum (Fall & Efstathiou 1980; MMW; Dalcanton, Spergel & Summers 1997). Since the time scale for new gas to reach the disk is never shorter than the free fall time, the formation of the resulting disk will cause a contraction of the dark matter halo that is close to adiabatic. In order to avoid contraction, one needs to abandon the idea that gas reaches the disk via a (relatively smooth) cooling flow. Rather, the disk material has to assemble out of several (massive) clumps, which reach the center of the halo by dynamical friction. After all, dynamical friction transfers the potential energy and orbital angular momentum of the clumps to the dark matter particles, which consequently move to larger radii (e.g., El-Zant, Shlosman & Hoffman 2001; Ma & Boylan-Kolchin 2004; Mo & Mao 2004; Tonini, Lapi & Salucci 2006). The same mechanism has also been proposed as an explanation for the large, constant density cores observed in some clusters of galaxies (El-Zant et al. 2004; Zapocosta et al. 2006).

In addition to providing a scenario for disk formation that

is consistent with the galaxy luminosity function, halo expansion may also help to alleviate a long-standing problem with observed rotation curves, which are claimed to be inconsistent with steeply cusped NFW profiles (e.g., Dutton et al. 2005 and references therein) and with the observed pattern speeds of bars (e.g., Debattista & Sellwood 2000, Weiner et al. 2001). Although we defer a detailed discussion on the rotation curve shapes of our various models to a forthcoming paper, we have verified that in all models discussed here the galaxies have realistic (i.e., flat) rotation curves.

Additional ‘support’ for Model IV comes from various estimates of the baryonic mass fractions of disk galaxies. As is evident from Fig.14, models with halo expansion that match the VL and RL zero points predict much lower values for λ_{gal} and m_{gal} than the standard models with adiabatic contraction. As we have argued above, there are several reasons for expecting $\lambda_{\text{gal}} < \lambda$. Support for low galaxy mass fractions comes from various sources, including the conditional luminosity function formalism (Yang et al. 2003, 2005; Cooray 2005) and galaxy-galaxy lensing (Guzik & Seljak 2002; Hoekstra et al. 2005). In particular, in one of the largest galaxy-galaxy lensing studies to date, Mandelbaum et al. (2006) find that late-type galaxies with a stellar mass of a few times $10^{10} h^{-1} M_{\odot}$, have on average, $m_{\text{gal}} \sim 0.03$ (i.e., corresponding to the parameter η in Mandelbaum et al. being 0.18), in good agreement with the value of $m_{\text{gal},0}$ for our Model IV.

The main potential problem for the ‘expansion-scenario’ proposed here is that it is not clear whether the merger between various clumps can produce a realistic disk galaxy. Although high resolution hydrodynamical simulations of disk formation in a cosmological framework have recently sug-

gested that realistic disk galaxies may form out of merging progenitors (e.g., Robertson et al. 2006), more work is clearly needed to investigate such a formation scenario in detail.

To summarize, if one is willing to abandon the idea that disk formation involves adiabatic contraction of the corresponding dark matter halo, one can construct disk formation models that simultaneously match the *VL* and *RL* relations using standard cosmological parameters. In addition, these model predict low baryonic mass fractions, in better agreement with the data, predict low spin parameters, consistent with a picture in which disks form preferentially in halos with quiescent merger histories, and, most importantly, yield characteristic values for $V_{2.2}/V_{\text{vir}}$ that suggest that one may be able to simultaneously fit the galaxy luminosity function.

6. SUMMARY

We have used the slopes, zero-points, and residuals of the observed *VL* and *RL* relations to place constraints on the standard Λ CDM-based model for the formation of disk galaxies. Our models consider exponential (baryonic) disks in centrifugal equilibrium within NFW dark matter halos. We model the reaction of the dark halo to disk formation in a way which permits it to range from the standard adiabatic contraction to an expansion of a similar magnitude. The disk stars-to-gas ratio is determined by a threshold surface density for star formation. A bulge is included based on a self-regulating mechanism that ensures disk stability. The disk properties are converted into observables using an empirically determined, luminosity-dependent, stellar mass-to-light ratio.

We construct samples of model galaxies including intrinsic scatter in halo concentrations, stellar mass-to-light ratios, and galaxy spin parameter. In addition, we mimic observational errors, and sample the model galaxies so that they reproduce the observed luminosity distribution. For each sample we construct model *VL* and *RL* relations which we compare to the data. By demanding the models to *simultaneously* reproduce the slopes, zero points and scatter of the observed *VL* and *RL* relations, including the correlation between the residuals, we obtain the following conclusions:

- Since the stellar mass-to-light ratio increases with increasing luminosity, the slopes of the *VL* and *RL* relations deviate from the basic halo virial relation $V_{\text{vir}} \propto R_{\text{vir}} \propto M_{\text{vir}}^{1/3}$. The observed *VL* slope is reproduced when the gas-to-stellar mass ratio is properly decreasing with mass. This is naturally achieved by a surface-density threshold for star formation. The observed *RL* slope requires that the disk mass fraction is properly increasing with mass, in agreement with generic predictions of supernova feedback (e.g., Dekel & Silk 1986; Dekel & Woo 2003).
- The standard model, assuming adiabatic contraction and Λ CDM halo concentrations, can match the *VL* zero point only with an unrealistically top-heavy IMF. Even in this case, the predicted ratio of $V_{2.2}/V_{\text{vir}}$ is too high for a match of the galaxy luminosity function.
- Models with a realistic IMF and adiabatic contraction require halo concentrations that are a factor two smaller than predicted, which is marginally consistent with the WMAP constraints on the cosmological parameters. Models with realistic IMFs and standard halo concentrations can simultaneously match the *VL* and *RL* zero points only if adiabatic contraction does not occur. In both of these cases the predicted ratio of $V_{2.2}/V_{\text{vir}}$ is too high for matching the luminosity function.
- If disk formation causes dark-matter halos to expand rather than contract, the *VL* and *RL* relations can be reproduced with standard halo concentrations combined with low values of galaxy spin parameter and mass fraction. The low average spin parameter is consistent with the picture in which disks survive in halos that have not experienced recent major mergers (D’Onghia & Burkert 2004). The low baryon fraction is consistent with galaxy-galaxy lensing studies (Mandelbaum et al. 2006). This model predicts that $V_{2.2} \simeq 1.2V_{\text{vir}}$, consistent with what is required to fit the luminosity function.
- The scatter in the *VL* relation has roughly equal contributions from scatter in c , in Υ_I and from observational errors. To match the amount of scatter observed, we require that $\sigma_{\ln c} \simeq 0.23$. This is smaller than the prediction for the full set of dark-matter halos, $\sigma_{\ln c} \simeq 0.32$ (Bullock et al. 2001a), but consistent with the sub-sample of halos without recent major mergers (Wechsler et al. 2002).
- The *RL* scatter is dominated by scatter in the spin parameter λ_{gal} . The observed *RL* scatter requires that $\sigma_{\ln \lambda} \simeq 0.25$, about half the value predicted for Λ CDM halos. This is again consistent with the picture in which disks survive in halos with a quiet merger history. This picture also implies that the *average* spin parameter is low. A simultaneous match of the *VL* and *RL* relations with such a low λ_{gal} requires that the baryonic mass fraction is also low. This, in turn, strongly favors a model with expansion rather than adiabatic contraction.
- The observed residuals of the *VL* and *RL* relations show only a weak anti-correlation. We have shown that this can partly be attributed to the threshold density for star formation, which causes the spread in λ_{gal} to scatter galaxies along the *VL* relation (see also FA00). Reproducing the shallow slope γ of the residual correlation is possible only when there is scatter in Υ_I and when the scatter in c is relatively low, $\sigma_{\ln c} \lesssim 0.23$.
- Unlike the earlier suggestion by Courteau & Rix (1999), we find that γ does not provide a strong constraint on the baryon fraction in the inner halo. The relation between γ and $V_{\text{gal}}/V_{2.2}$ depends on several model ingredients such as the degree of halo contraction or expansion, the threshold density for star formation, and the sensitivity of γ to the scatter in the different variables. In addition, in all our models there is a large scatter in $V_{\text{gal}}/V_{2.2}$ which is strongly correlated with surface brightness. This correlation results in the highest surface brightness galaxies being baryon within 2.2 disk scale lengths, while at the same time allowing the lowest surface brightness galaxies to be dark matter dominated as is generally accepted.
- Although observations have shown that the *VL* and *RL* residuals are uncorrelated, our models robustly predict that the residuals of the *baryonic VM* and *RM* relations are strongly anti-correlated.

Based on these results we conclude that the standard model, which includes standard adiabatic contraction, standard halo concentration parameters and a standard IMF, does not allow a simultaneous match to the *VL* and *RL* relations. This is a modification of earlier conclusions, e.g., by MMW and Pizagno et al. (2005), which owes to our more realistic modeling (see Appendix A). Although a proper fit can be obtained if the halo concentrations are significantly lower, or if adiabatic contraction does not occur, these models predict high values of $V_{2,2}/V_{\text{vir}}$ which prevent a match with the galaxy luminosity function. They also predict high baryonic mass fractions in conflict with results from galaxy-galaxy lensing.

To circumvent these problems, we advocate a model in which the dark matter halo responds by expansion rather than by contraction, to the formation of the disk. This model (i) predicts values for $V_{2,2}/V_{\text{vir}}$ that allow a simultaneous fit to the LF (ii) is consistent with disks forming predominantly in dark matter halos that have not experienced a recent major merger, (iii) predicts low baryonic mass fractions, in agreement with a wide range of observations, and (iv) predicts dark matter halos that are less centrally concentrated, in better agreement with rotation curve shapes and bar pattern speeds.

The idea of an expanding dark matter halo is counter to the standard model for disk formation, in which disks form out of relatively smooth cooling flows that conserve their specific angular momentum. Rather, the expansion scenario requires that disks form out of merging clumps, which transfer energy and angular momentum to the dark matter via dynamical friction and three body interactions. Such a scenario naturally arises if disks form out of clumpy, cold accretion flows (Birnboim & Dekel 2003; Keres et al. 2005; Dekel & Birnboim 2006). While the formation of realistic disk galaxies out of such clumpy streams is yet to be investigated in detail, preliminary hints are provided by hydrodynamical simulations which have demonstrated that disks can originate from merging gaseous progenitors (e.g., Robertson et al. 2006).

We thank E. Bell, S.M. Faber, A. Maller & B. Robertson for stimulating discussions. A.A.D. has been partly supported by the Swiss National Science Foundation (SNF). A.D. has been partly supported by ISF 213/02, NASA ATP NAG5-8218, a Miller Professorship at UC Berkeley, and a Blaise Pascal International Chair in Paris. S.C. acknowledges the support of NSERC through a Discovery grant.

REFERENCES

Avila-Reese, V., & Firmani, C. 2000, Revista Mexicana de Astronomia y Astrofisica, 36, 23

Avila-Reese, V., Firmani, C., & Hernández, X. 1998, ApJ, 505, 37

Bailin, J., Power, C., Gibson, B. K., Steinmetz, M. 2005a, preprint (astro-ph/0502231)

Bailin, J., et al. 2005b, ApJ, 627, L17

Bell, E. F., & de Jong, R. S. 2001, ApJ, 550, 212

Bell, E. F., McIntosh, D. H., Katz, N., & Weinberg, M. D. 2003a, ApJS, 149, 289

Bell, E. F., Baugh, C. M., Cole, S., Frenk, C. S., & Lacey, C. G. 2003b, MNRAS, 343, 367

Benson, A. J., Bower, R. G., Frenk, C. S., Lacey, C. G., Baugh, C. M., & Cole, S. 2003, ApJ, 599, 38

Binney, J., & Tremaine, S. 1987, Princeton, NJ, Princeton University Press, 1987, 747 p..

Birnboim, Y., & Dekel, A. 2003, MNRAS, 345, 349

Blumenthal, G. R., Faber, S. M., Flores, R., & Primack, J. R. 1986, ApJ, 301, 27

Bottema, R. 1993, A&A, 275, 16

Bryan, G. L., & Norman, M. L. 1998, ApJ, 495, 80

Bullock, J. S., Kolatt, T. S., Sigad, Y., Somerville, R. S., Kravtsov, A. V., Klypin, A. A., Primack, J. R., & Dekel, A. 2001a, MNRAS, 321, 559

Bullock, J. S., Dekel, A., Kolatt, T. S., Kravtsov, A. V., Klypin, A. A., Porciani, C., & Primack, J. R. 2001b, ApJ, 555, 240

Chen, D. N., Jing, Y. P., & Yoshikawa, K. 2003, ApJ, 597, 35

Christodoulou, D. M., Shlosman, I., & Tohline, J. E. 1995, ApJ, 443, 551

Cole, S., Aragon-Salamanca, A., Frenk, C. S., Navarro, J. F., & Zepf, S. E. 1994, MNRAS, 271, 781

Cole, S., Lacey, C. G., Baugh, C. M., & Frenk, C. S. 2000, MNRAS, 319, 168

Cooray, A. 2005, MNRAS, 363, 337

Courteau, S. 1996, ApJS, 103, 363

Courteau, S. 1997, AJ, 114, 2402

Courteau, S., de Jong, R. S., & Broeils, A. H. 1996, ApJ, 457, L73

Courteau, S., & Rix, H. 1999, ApJ, 513, 561

Courteau, S., Willick, J. A., Strauss, M. A., Schlegel, D., & Postman, M. 2000, ApJ, 544, 636

Courteau, S., Dutton, A. A., van den Bosch, F., Dekel, A., MacArthur, L. A., McIntosh, D. H., & Dale, D. 2006, submitted to ApJ

Croton, D. J., et al. 2006, MNRAS, 365, 11

Dalcanton, J. J., Spergel, D. N., & Summers, F. J. 1997, ApJ, 482, 659

Dale, D. A., Giovanelli, R., Haynes, M. P., Campusano, L. E., & Hardy, E. 1999, AJ, 118, 1489

Debattista, V. P., & Sellwood, J. A. 2000, ApJ, 543, 704

Debattista, V. P., Mayer, L., Carollo, C., Moore, B., Wadsley, J., & Quinn, T. 2006, ApJ, 645, 209

de Jong, R. S. 1996, A&A, 313, 377

de Jong, R. S., & Lacey, C. 2000, ApJ, 545, 781

Dekel, A., & Silk, J. 1986, ApJ, 303, 39

Dekel, A., & Woo, J. 2003, MNRAS, 344, 1131

Dekel, A., & Birnboim, Y. 2006, MNRAS, 368, 2

D'Onghia, E., & Burkert, A. 2004, ApJ, 612, L13

Dutton, A. A., Courteau, S., de Jong, R., & Carignan, C. 2005, ApJ, 619, 218

Eisenstein, D. J., & Loeb, A. 1996, ApJ, 459, 432

Eke, V. R., Navarro, J. F., & Steinmetz, M. 2001, ApJ, 554, 114

Elizondo, D., Yepes, G., Kates, R., Müller, V., & Klypin, A. 1999, ApJ, 515, 525

El-Zant, A. A., Shlosman, I., & Hoffman, Y. 2001, ApJ, 560, 636

El-Zant, A. A., Hoffman, Y., Primack, J., Combes, F., & Shlosman, I. 2004, ApJ, 607, L75

Fall, S. M., & Efstathiou, G. 1980, MNRAS, 193, 189

Firmani, C., & Avila-Reese, V. 2000, MNRAS, 315, 457 (FA00)

Freeman, K. C. 1970, ApJ, 160, 811

Ghigna, S., Moore, B., Governato, F., Lake, G., Quinn, T., & Stadel, J., 1998, MNRAS, 300, 146

Giovanelli, R., Haynes, M. P., Salzer, J. J., Wegner, G., da Costa, L. N., & Freudling, W. 1994, AJ, 107, 2036

Giovanelli, R., Haynes, M. P., Herter, T., Vogt, N. P., da Costa, L. N., Freudling, W., Salzer, J. J., & Wegner, G. 1997, AJ, 113, 53 (G97)

Gnedin, O. Y., Kravtsov, A. V., Klypin, A. A., & Nagai, D. 2004, ApJ, 616, 16

Guzik, J., & Seljak, U. 2002, MNRAS, 335, 311

Heavens, A. F., & Jimenez, R. 1999, MNRAS, 305, 770

Hernquist, L. 1990, ApJ, 356, 359

Hoekstra, H., Hsieh, B. C., Yee, H. K. C., Lin, H., & Gladders, M. D. 2005, ApJ, 635, 73

Hohl, F. 1971, ApJ, 168, 343

Kannappan, S. J. 2004, ApJ, 611, L89

Kauffmann, T., Mayer, L., Wadsley, J., Stadel, J., & Moore, B. 2006, MNRAS, 370, 1612

Kauffmann, G., et al. 2003a, MNRAS, 341, 33

Kauffmann, G., et al. 2003b, MNRAS, 341, 54

Kauffmann, G., White, S. D. M., & Guiderdoni, B. 1993, MNRAS, 264, 201

Kennicutt, R. C. 1983, ApJ, 272, 54

Kennicutt, R. C. 1989, ApJ, 344, 685

Kennicutt, R. C. 1998, ApJ, 498, 541

Keres, D., Katz, N., Weinberg, D. H., & Davé R. 2005, MNRAS, 363, 2

Kogut, A., et al. 1993, ApJ, 419, 1

Li, Y., Mo, H. J., van den Bosch, F. C. 2005, preprint (astro-ph/0510372)

Ma, C., & Boylan-Kolchin, M. 2004, Physical Review Letters, 93, 021301

MacArthur, L. A., Courteau, S., & Holtzman, J. A. 2003, ApJ, 582, 689

Macciò, A. V., Dutton, A. A., van den Bosch, F. C., Moore, B., Potter, D., & Stadel, J. G. 2006, pre-print (arXiv:astro-ph/0608157)

Maller, A. H., & Bullock, J. S. 2004, MNRAS, 355, 694

Mandelbaum, R., Seljak, U., Kauffmann, G., Hirata, C. M., & Brinkmann, J. 2006, MNRAS, 368, 715

Mathewson, D. S., Ford, V. L., & Buchhorn, M. 1992, ApJS, 81, 413

McGaugh, S. S., & de Blok, W. J. G. 1997, ApJ, 481, 689

McGaugh, S. S., Schombert, J. M., Bothun, G. D., & de Blok, W. J. G. 2000, ApJ, 533, L99

McGaugh, S. S. 2005, Phys. Rev. Lett, 95, 1302

Mo, H. J., Mao, S., & White, S. D. M. 1998, MNRAS, 295, 319 (MMW)

Mo, H. J., & Mao, S. 2000, MNRAS, 318, 163

Mo, H. J., & Mao, S. 2004, MNRAS, 353, 829

Natarajan, P. 1999, ApJ, 512, L105

Navarro, J. F., Frenk, C. S., & White, S. D. M. 1997, ApJ, 490, 493

Navarro, J. F., & Steinmetz, M. 2000, ApJ, 538, 477

Norman, C. A., Sellwood, J. A., & Hasan, H. 1996, ApJ, 462, 114

O'Neill, J. K., & Dubinski, J. 2003, MNRAS, 346, 251

Pizagno, J., et al. 2005, ApJ, 633, 844

Portinari, L., Sommer-Larsen, J., & Tantalo, R. 2004, MNRAS, 347, 691

Robertson, B., Bullock, J. S., Cox, T. J., Di Matteo, T., Hernquist, L., Springel, V., & Yoshida, N. 2006, ApJ, 645, 986

Salpeter, E. E. 1955, ApJ, 121, 161

Schlegel, D. J., Finkbeiner, D. P., & Davis, M. 1998, ApJ, 500, 525

Sharma, S., & Steinmetz, M. 2005, ApJ, 628, 21

Shen, S., Mo, H. J., White, S. D. M., Blanton, M. R., Kauffmann, G., Voges, W., Brinkmann, J., & Csabai, I. 2003, MNRAS, 343, 978

Silk, J. 1997, ApJ, 481, 703

Somerville, R. S., & Primack, J. R. 1999, MNRAS, 310, 1087

Sommer-Larsen, J., Götz, M., & Portinari, L. 2003, ApJ, 596, 47

Spergel, D. N., et al. 2003, ApJS, 148, 175

Spergel, D. N., et al. 2006, preprint (astro-ph/0603449)

Tonini, T., Lapi, A., & Salucci, P. 2006, preprint (astro-ph/0603051)

Toomre, A. 1964, ApJ, 139, 1217

Tully, R. B., & Fisher, J. R. 1977, A&A, 54, 661

Tully, R. B., Pierce, M. J., Huang, J., Saunders, W., Verheijen, M. A. W., & Witchalls, P. L. 1998, AJ, 115, 2264

Valenzuela, O., & Klypin, A. 2003, MNRAS, 345, 406

van Albada, T. S., Bahcall, J. N., Begeman, K., & Sancisi, R. 1985, ApJ, 295, 305

van den Bosch, F. C. 1998, ApJ, 507, 601

van den Bosch, F. C. 2000, ApJ, 530, 177

van den Bosch, F. C. 2001, MNRAS, 327, 1334

van den Bosch, F. C. 2002, MNRAS, 332, 456

van den Bosch, F. C., Lewis, G. F., Lake, G., & Stadel, J., 1999, ApJ, 515, 50

van den Bosch, F. C., Robertson, B. E., Dalcanton, J. J., & de Blok W. J. G. 2000, AJ, 119, 1579

van den Bosch, F. C., Abel, T., Croft, R. A. C., Hernquist, L., & White, S. D. M. 2002, ApJ, 576, 21

van den Bosch, F. C., Mo, H. J., & Yang, X. 2003, MNRAS, 345, 923

Wechsler, R. H., Bullock, J. S., Primack, J. R., Kravtsov, A. V., & Dekel, A. 2002, ApJ, 568, 52

Weinberg, M. D. 1985, MNRAS, 213, 451

Weiner, B. J., Sellwood, J. A., & Williams, T. B. 2001, ApJ, 546, 931

Willick, J. A., Courteau, S., Faber, S. M., Burstein, D., Dekel, A., & Strauss, M. A. 1997, ApJS, 109, 333

Wilson, G. M. 2003, PhD Thesis, The Australian National University

Yang, X., Mo, H. J., & van den Bosch, F. C. 2003, MNRAS, 339, 1057

Yang, X., Mo, H. J., Jing, Y. P., & van den Bosch, F. C. 2005, MNRAS, 358, 217

Zappacosta, L., Buote, D. A., Gastaldello, F., Humphrey, P. J., Bullock, J., Brighenti, F., & Mathews W. 2006, preprint (astro-ph/0602613)

Zavala, J., Avila-Reese, V., Hernández-Toledo, H., & Firmani, C. 2003, A&A, 412, 633

Zentner, A. R., & Bullock, J. S. 2002, Phys. Rev. D, 66, 043003

Zhao, D. H., Mo, H. J., Jing, Y. P., Börner, G. 2003, MNRAS, 339, 12

APPENDIX

A: COMPARISON WITH PIZAGNO ET AL. 2005

Pizagno et al. (2005, hereafter P05) study the correlations among stellar mass, M_* , I -band disk scale length, R_I , and rotation velocity at 2.2 disk scale lengths, $V_{2.2}$, for a sample of 81 disk dominated galaxies (defined to have disk-to-total luminosity fractions greater than 0.9). In what follows we refer to the $V_{2.2}-M_*$ and R_I-M_* relations as the VM and RM relations, respectively. P05 estimate stellar masses using $g-r$ colors corrected for extinction and the relations in Bell et al. (2003a). As shown in §3.4 the Υ_I-L_I relation of P05 is in excellent agreement with ours (assuming the same IMF).

P05 claim that a MMW model with $m_d = 0.05$, $\lambda = 0.06$, $c_{200} = 10$ and using the adiabatic contraction formula of Gnedin et al. (2004) matches the VM and RM data reasonably well. This is in disagreement with our statement that the MMW model is unable to reproduce the slopes of the VL and RL relations (§4.1.1) and with our claim that models with adiabatic contraction, standard halo concentrations, and standard IMFs require $m_{\text{gal}} \simeq \lambda_{\text{gal}} \simeq 0.1$ in order to match the VL zero point (Fig. 14). Below we address these and other differences between our results and those of P05.

- We first note that unlike our VL relation and those of Giovanelli et al. 1997, the VM and VL relations of P05 do not follow a single power-law. There is a significant deviation below $V_{2.2} = 120 \text{ km s}^{-1}$ in both their VM and VL relations. In what follows we focus on their galaxies with $V_{2.2} > 120 \text{ km s}^{-1}$.
- P05 assume $c_{200} = 10$ and that the disk is 100% stars, thus their VM relation has a slope of $1/3$, in agreement with their data. However, as shown in §4.1.1, the expected variation of c and the gas-to-stellar mass ratio with M_{vir} both result in significantly shallower VM slopes. Thus either c and the gas-to-stellar mass ratio do not depend significantly on M_{vir} , or their data significantly over-estimates the VM slope.
- As can clearly be seen in Fig. 4 of P05, their model with $m_d = 0.05$ and $\lambda = 0.06$ does not match the VM zero point of the data. Their model with $m_d = 0.10$ and $\lambda = 0.08$ provides a better match, but predicts a much stronger dependence of VM scatter on λ , and hence disk size. Their models assume pure stellar disks. Including reasonable gas-to-stellar mass ratios requires even larger values of m_d and λ to match the VM zero point which are now consistent with our results (see Fig. 14).
- P05 do not construct a self consistent model for the VM and RM relations and their scatter. We have verified that pure disk models (e.g. MMW) which simultaneously match the VM and RM relations *always* predict a significant correlation between VM and RM residuals. P05 speculated that a weak correlation between size and VM residual could be washed out by other sources that contribute to the VM scatter. However the only significant sources to the VM scatter are c and observational errors. We have found that while observational errors do reduce the strength of the residual correlation the effect is small. By contrast scatter in c results in a significantly stronger negative correlation between the residuals. Thus rather than washing out the correlation between size and VM residual, the expected scatter in c and observational errors will result in a stronger correlation.
- The RL relation of P05, as shown in Fig. 3, has a significantly higher zero point normalization than ours. The most likely sources of this difference are their bulge-to-disk ratio selection criteria, or their lack of inclination corrections to the disk sizes. Their larger disk sizes require a $\simeq 50\%$ larger spin parameter, λ_{gal} , assuming all the other model parameters are kept fixed. Larger disks, at a given disk mass, contribute less to $V_{2.2}$, and result in less halo contraction. This makes it easier to fit the VL zero point and also weakens the correlation between the VL and RL residuals. However, as can be seen in Fig. 14 even a 50% increase in the RL zero point (corresponding to about 1σ of the observational scatter) would not significantly change any of our conclusions regarding a simultaneous match of the VL and RL zero points and a low ratio of $V_{2.2}/V_{\text{vir}}$.

In summary, although there are differences in the data samples used by P05 and ourselves, both our and the P05 data require large $m_{\text{gal}} \simeq \lambda_{\text{gal}} \simeq 0.1$ in order to match the VL zero point. Not only is such a high value of λ_{gal} unrealistic, such a high m_{gal} is also inconsistent with galaxy-galaxy lensing constraints. Furthermore the MMW model adopted by P05 is unable to reproduce the slope or the surface brightness independence of the VL relation, due to the overly simplistic assumption that galaxy disks are 100% stars.

B: CORRELATIONS BETWEEN MODEL PARAMETERS

We have assumed that the scatter in the model parameters are uncorrelated. For completeness, we here present a brief discussion on how correlations between model parameters might affect our results.

- $\lambda-c$ anti-correlation: Bullock et al. (2001b) found no correlation between λ and c above the weak correlation expected from the definition of λ . However, Bailin et al. (2005a) claim a correlation, but this is likely due to their inclusion of unrelaxed halos (Macciò et al. 2006). Suppose halos with larger λ have lower c ; looking at Fig. 7 we see that this would result in larger scatter in both the RL and VL relations, and by the same reasoning a stronger residual correlation.
- Υ_I-c correlation: At a fixed halo mass, lower c halos assemble later; in addition lower c halos result in lower surface density disks. Thus, everything else being equal, we expect that at a fixed halo mass, lower c halos to contain galaxies with younger (bluer) stellar populations than halos with larger c . Since younger populations correspond to lower stellar mass-to-light ratios, we thus expect a positive correlation between c and Υ_I . From Fig. 7 we see that such a correlation increases the overall VL scatter. It will also decrease the RL scatter, but since Υ_I and c contribute relatively little to the RL scatter, this reduction is unlikely to be significant.

- $\lambda_{\text{gal}} - m_{\text{gal}}$ correlation: since mass is more centrally concentrated than specific angular momentum one generally expects that $j_{\text{gal}} < m_{\text{gal}}$ if disk galaxies form inside out. This implies that a smaller m_{gal} implies a smaller λ_{gal} . If these two parameters are indeed positively correlated, the overall scatter in the RL relation is predicted to be smaller, as can be seen from Fig. 7. However, recall (§4.1 & 4.3) that it is the correlation between the gas-to-stellar mass ratio and λ_{gal} , through a critical star formation threshold density, that is essential in reproducing the slope of the VL relation and the surface brightness independence of the VL relation. Any models that introduce a correlation between λ_{gal} and m_{gal} will likely erase these successes.
- $\Upsilon - \lambda_{\text{gal}}$ anti-correlation: At a fixed baryonic mass lower λ_{gal} results in higher surface density disks. Since empirically the star formation efficiency is proportional to the surface density of the stars (Kennicutt 1998), we thus expect higher surface density systems to have older stellar populations, in agreement with the data (Kauffmann et al. 2003b). Such an anti-correlation would tend to remove any color dependence of the RL relation and hence reduce its scatter (Bell et al. 2003b). However, it would also increase the surface brightness dependence of the VL relation.

In summary, there are several plausible correlations between model parameters. Although three of these have the potential to explain why the RL scatter is smaller than predicted, we do not expect that these correlations can reconcile the full amount of scatter in λ expected from simulations with the observed scatter in the RL relation. Furthermore, each of these correlations will increase the strength of the correlation between VL and RL residuals (or equivalently the strength of the surface brightness dependence of the VL relation). Thus to reproduce the weakly correlated residuals we would require even less scatter in c than the $\sigma_{\ln c} = 0.23$ we currently adopt. This reinforces the conclusion that disk galaxies form in a subset of halos.

C: COURTEAU & RIX (1999) REVISITED

CR99 argued that the weak correlation between the residuals of the VL and RL relations, $\gamma \simeq -0.1$, implies disks of high surface brightness galaxies should have, *on average* $V_d/V_{2.2} \simeq 0.6$. CR99 arrive at this result by computing $\partial \log V_{2.2} / \partial \log R_d$ for models consisting of exponential disks in NFW halos with adiabatic contraction. They found that in these models $\partial \log V_{2.2} / \partial \log R_d$ correlates with $V_d/V_{2.2}$ (the ratio of the circular velocity of the disk to the total circular velocity, at 2.2 disk scale lengths), such that galaxies with higher $V_d/V_{2.2}$ have more negative $\partial \log V_{2.2} / \partial \log R_d$, with the limiting case of $\partial \log V_{2.2} / \partial \log R_d = -0.5$ for a pure exponential disk. Thus by assuming that $\partial \log V_{2.2} / \partial \log R_d$ is equivalent to the observed slope of the residual correlation γ , they concluded that $V_d/V_{2.2} \simeq 0.6$. This would suggest more DM than baryons within 2.2 disk scale lengths, but not that the baryon contribution is insignificant. If the baryons were insignificant then the CR99 model would predict $\partial \log V_{2.2} / \partial \log R_d > 0$. However, as outlined below, several of the assumptions made in CR99 are not true in general.

- CR99 assumed that halos contract adiabatically to the formation of the disk. In Fig. 16, which should be compared with Fig. 9 of CR99, we repeat the CR99 analysis for halos with and without adiabatic contraction. Note that CR99 used $c_{200} = 10$ and that $c_{\text{vir}} \simeq 1.3 c_{200}$, for ease of comparison we also adopt their definition here. We see that turning off adiabatic contraction increases $V_d/V_{2.2}$ by about 30% at a fixed $\partial \log V_{2.2} / \partial \log R_d$.
- CR99 assumed that bulge formation does not affect the scale length of the disk. We have shown that in models where the specific angular momentum of the disk increases due to bulge formation (e.g. $f_x = 0.25$) the residual correlation is weakened.
- CR99 assumed that the contribution of the gas to the disk is negligible. While this is true for the highest surface brightness galaxies, moderate surface brightness galaxies contain more gas. We have shown (see §4.3) that the correlation between the gas-to-stellar mass ratio and disk surface density significantly reduces the strength of the residual correlations.
- CR99 underplayed the effect of scatter in halo concentration c and stellar mass-to-light ratio Υ . Fig. 12 shows that scatter in these parameters can result in significantly different residual correlation slopes. Scatter in c results in a more negative correlation while scatter in Υ results in a more positive correlation. For realistic amounts of scatter in both c and Υ the residual correlation is weakened.
- CR99 assumed that $\gamma \equiv \partial \log V_{2.2} / \partial \log R_d$. In general this is not true, because γ is a global quantity while $\partial \log V_{2.2} / \partial \log R_d$ is a local quantity. More specifically γ is the slope of the VL and RL residuals for a sample of galaxies, while $\partial \log V_{2.2} / \partial \log R_d$ is the slope of the change in V due to change in R , at fixed disk mass, for a single galaxy.

Thus we conclude that the VL - RL residuals cannot be used to place model independent constraints on the baryonic fraction of disk galaxies. However, this does not diminish their importance as a constraint for galaxy formation models.

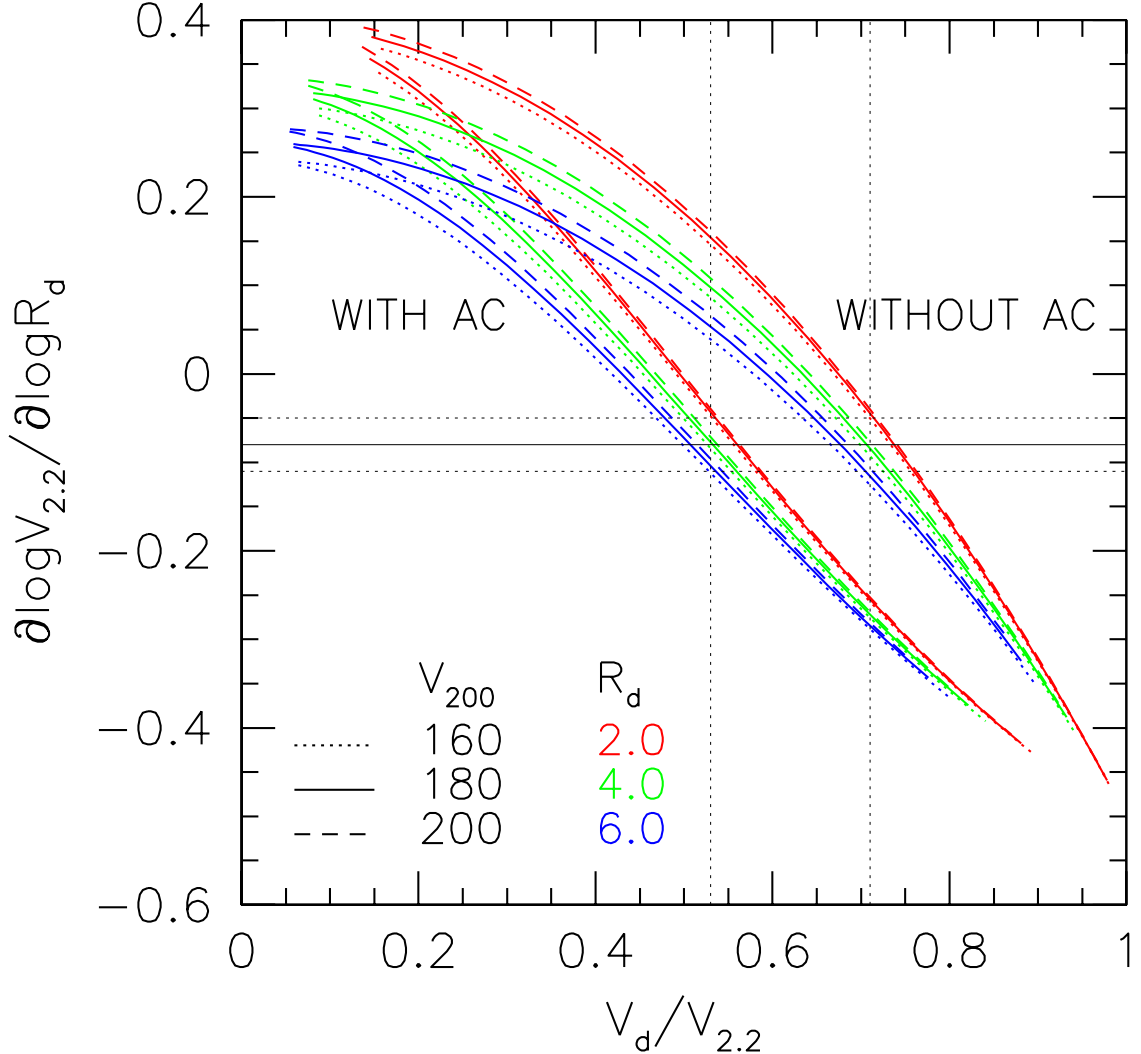


FIG. 16.— CR99 analysis for NFW halos with $c_{200} = 10$ with and without adiabatic contraction (AC). Note that $c_{vir} \simeq 1.3c_{200}$. The y-axis shows the change in $\log V_{2.2}$ due to changes in $\log R_d$ at fixed M_d . The line and color types correspond to different values of V_{200} and R_d , respectively, as indicated in the figure. The horizontal solid and dotted lines show the observed slope of the $\Delta \log V - \Delta \log R$ relation. The vertical dotted lines show the $V_d/V_{2.2}$ corresponding to the $V_{200} = 180, R_d = 4$ models. Models without AC have a substantially larger $V_d/V_{2.2}$ (about 30%) than models with AC.